

# Treatment of Ionospheric Effects in Single and Dual Frequency GNSS Receivers for Satellite Applications

Manuel Hahn

Master of Science  
Space Engineering - Space Master

Luleå University of Technology  
Department of Computer Science, Electrical and Space Engineering

LULEÅ UNIVERSITY OF TECHNOLOGY

MASTER'S THESIS

TREATMENT OF IONOSPHERIC EFFECTS IN SINGLE  
AND DUAL FREQUENCY GNSS RECEIVERS  
FOR SATELLITE APPLICATIONS

MANUEL HAHN

OCTOBER 2011

## Abstract

The present work deals with the treatment of ionospheric effects in single and dual frequency GNSS receivers for satellite applications in general and the application of selected ionospheric correction algorithms to Astrium's MosaicGNSS receiver in particular. Currently, the MosaicGNSS receiver provides a 3D position error RMS of 10 m that is supposed to be improved by the ionospheric correction algorithms.

For single-frequency applications, three algorithms based on ionospheric models are chosen to be analyzed, i.e. the Lear model, the Klobuchar model and the Montenbruck model. Additionally, the GRAPHIC code / DRVID technique is selected for analysis that uses code and carrier-phase of the L1 signal to calculate the ionospheric path delay. For dual-frequency applications, the ionospheric error is directly calculated by use of P1 and P2 pseudorange measurements. These algorithms are implemented in the MosaicGNSS receiver, tested and finally validated by use of real flight data from the CHAMP mission. Additionally, several data editing techniques are developed that are specifically tailored to exclude invalid or degraded measurements from the navigation solution.

By applying a strategy that consists of selecting the ionospheric correction algorithm depending on the long-term solar activity, a 3D position error RMS of 3.45 - 6.63 m can be achieved.

## **Acknowledgments**

First of all I want to thank the GeoForschungsZentrum Potsdam for providing CHAMP/GPS data through their Information System and Data Center.

At EADS Astrium, I want to thank Dr. Christoper Kühn for giving me the opportunity to carry out this Master's thesis. Special thanks goes to Hannes Filippi and Andrés Barrios-Montalvo for their continuous support during the entire thesis. Carsten Müller I want to thank for great discussions and enlightening comments.

At the Université Paul Sabatier Toulouse III, I want to thank Christophe Peymirat for his great support in all situations. At the Luleå University of Technology, special thanks goes to Dr. Victoria Barabash, Anette Snällfot-Brändström and Maria Winnebäck for the organization of the SpaceMaster programme.

My parents I want to thank for their everlasting and undivided help and support. Finally, I want to thank Ania for her great support and patience during the preparation of this thesis.

# Table of Contents

<b>1</b>	<b>Introduction</b>	<b>1</b>
1.1	Master thesis description . . . . .	1
1.2	Tasks description and planning . . . . .	1
<b>2</b>	<b>Background information</b>	<b>4</b>
2.1	Precise real-time orbit determination . . . . .	4
2.2	GNSS receivers . . . . .	6
2.3	The Ionosphere and its influence on GNSS receivers . . . . .	9
<b>3</b>	<b>Requirement analysis and -specification</b>	<b>13</b>
3.1	Functional requirements . . . . .	13
3.2	System analysis . . . . .	13
3.3	Functional specification . . . . .	15
<b>4</b>	<b>System design and - specification</b>	<b>19</b>
4.1	Klobuchar model . . . . .	19
4.2	Lear & Lear/Klobuchar model . . . . .	21
4.3	Montenbruck model . . . . .	23
4.4	GRAPHIC/DRVID . . . . .	25
4.5	Dual-frequency correction . . . . .	28
4.6	Data editing . . . . .	30
4.7	Summary . . . . .	31
<b>5</b>	<b>Implementation and testing</b>	<b>32</b>
5.1	MosaicGNSS receiver . . . . .	32
5.2	CHAMP mission . . . . .	32
5.3	Matlab/Simulink environment . . . . .	33
5.4	Testing . . . . .	34
<b>6</b>	<b>Evaluation</b>	<b>35</b>
6.1	Selected GPS data sets . . . . .	35
6.2	Data editing analysis . . . . .	36

6.3 Ionospheric path delay analysis . . . . .	37
6.4 Navigation solution analysis . . . . .	42
<b>7 Concluding remarks</b>	<b>47</b>
<b>References</b>	<b>49</b>
<b>List of figures</b>	<b>51</b>

# Introduction

## 1.1 Master thesis description

In today's GNSS receivers the ionospheric effect is one of the major error sources. Due to a change in the refraction index, the signals passing through the ionosphere are altered w.r.t. their code and carrier. Several options exist for reducing the impact on the navigation:

- modeled corrections
- single frequency corrections, using Code and carrier phase
- dual (multiple) frequency corrections

The task of this Master thesis is to review the models used in Astrium's MosaicGNSS receiver, to assess single and dual frequency based estimations of the ionospheric delay and to suggest algorithms which can be implemented on board. The suggested algorithms are to be implemented and to be validated either in a Matlab/Simulink based simulation environment or on a receiver's laboratory model, pending the availability of real hardware.

The results of the Master thesis are planned to be included in the improvement process of Astrium's navigation receivers to reduce the impact of ionospheric variations on the navigation performance.

The Master thesis is carried out at EADS Astrium, Ottobrunn/Germany under supervision of Dr. Christopher Kühl.

## 1.2 Tasks description and planning

1. Familiarization with the topic including a literature survey concerning GNSS receivers in general and ionospheric effects in particular (2 weeks)

- ⇒ Product: Literature survey memo
- 2. Requirement analysis and - specification (2.5 weeks in total)
  - (a) Review of the Astrium's MosaicGNSS receiver software (1 week)
  - (b) Review of the Matlab/Simulink based simulation environment (1 week)
 ⇒ Product: Requirement specification document
- 3. System design and - specification (4.5 weeks in total)
  - (a) Assessment of single and dual frequency based estimations of the ionospheric delay (3 weeks)
  - (b) Suggestion of algorithms that can be implemented onboard (1 week)
 ⇒ Product: Design specification document
- 4. Implementation of suggested algorithms including source code documentation and functional tests (3 weeks)
  - ⇒ Product: Final version of code for algorithms
- 5. Validation of suggested algorithms (5 weeks in total)
  - (a) Testing with Matlab/Simulink based simulation environment (1 week)
  - (b) Review a receiver's laboratory model (1 week)
  - (c) Testing with a receiver's laboratory model (1 week)
  - (d) Testing with real flight data (1 week)
  - (e) Evaluation of results (1 week)
 ⇒ Product: Algorithms evaluation document
- 6. Completion of documentation including compilation of Master thesis (2 weeks)
  - ⇒ Product: Final version of Master thesis

The estimated total amount of time needed for the completion of the Master thesis is 19 weeks. By adding a security buffer of 2 weeks, a total duration from week 13 (28.03.2011) to week 33 (19.08.2011) is obtained.

A time schedule in form of a Gantt diagram can be found in figure 1.1.

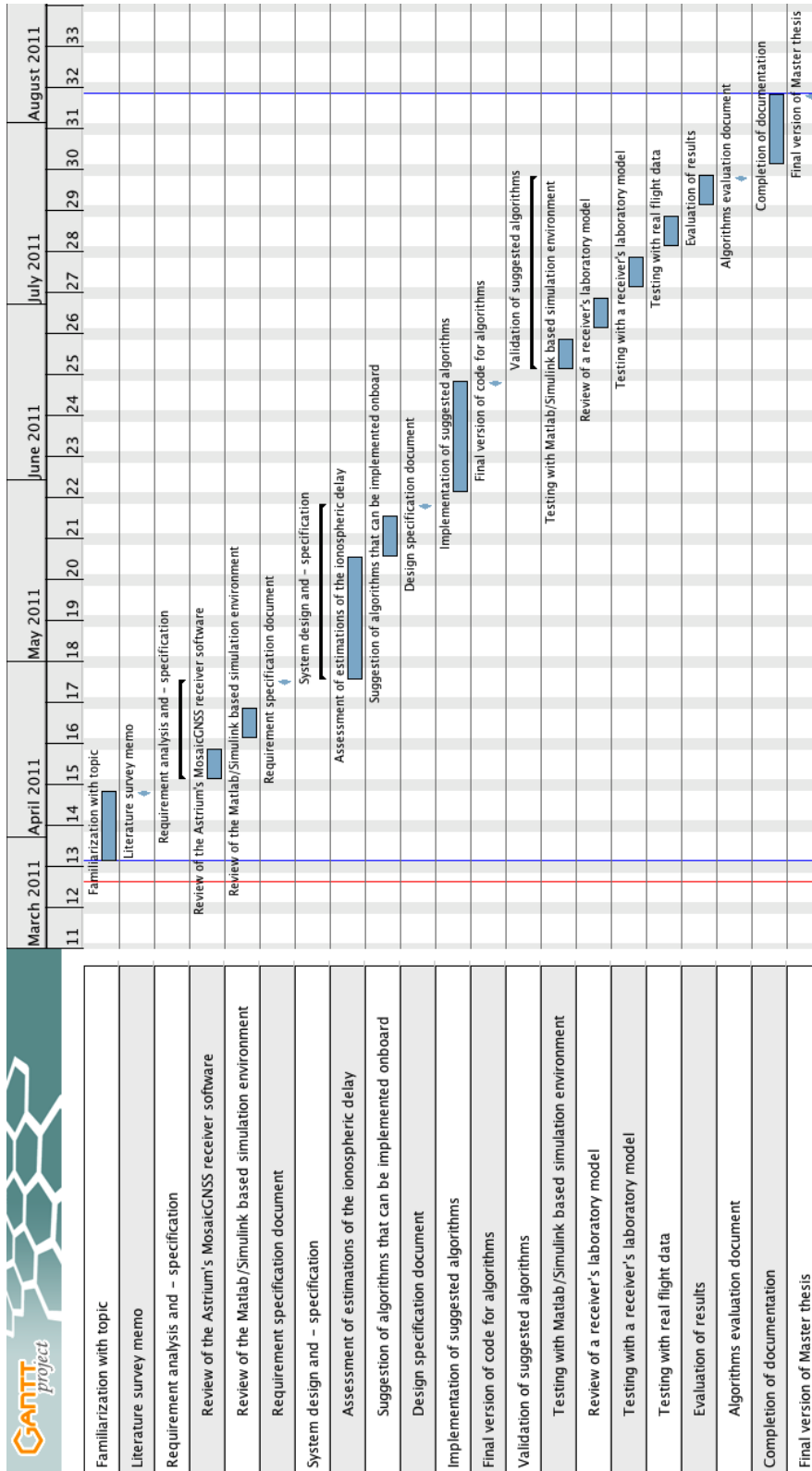


Figure 1.1: Time schedule for Master thesis

# Background information

This chapter is basically a summary of [1, 2] and explains the basic concepts relevant for understanding the Master thesis' topic. It shall help the reader getting an overview of precise real-time orbit determination, GNSS receivers and the impact of the ionosphere on the GNSS signal. This finally yields to the topic of the Master thesis, the treatment of ionospheric effects in GNSS receivers, what will then be discussed in detail in the following chapters.

## 2.1 Precise real-time orbit determination

Once placed on an orbit around Earth, a satellite's position and velocity change with time due to perturbing forces. Figure 2.1 gives an overview of the various perturbations that exist and their influence (in terms of acceleration) on the satellite's orbit. The perturbation's impact on the orbit, i.e. the acceleration that they cause on the satellite, depends on many different factors. The gravitational acceleration for example is dependent on the distance from satellite to the particular gravitational object like planets, Sun or Moon (in figure 2.1 the term GM refers to the Earth gravitational acceleration). Solar radiation pressure is a function of for example the satellite's mass and surface. The acceleration caused by atmospheric drag is dependent on the satellite's mass, surface and velocity as well as on the atmospheric density. The atmospheric density itself changes with the distribution of chemical constituents in the atmosphere, with the atmosphere's temperature and in general with altitude as well as with solar radiation effects (see chapter 2.3 for further details). The atmospheric drag represents the largest non-gravitational perturbation acting on LEO (Low-Earth-Orbit) satellites (as can be seen in figure 2.1). [1]

Due to these perturbations (mainly due to atmospheric drag), a satellite in LEO continuously loses altitude and spirals onto Earth until it finally burns on re-entry or falls on Earth's surface after only a few years (depending on starting

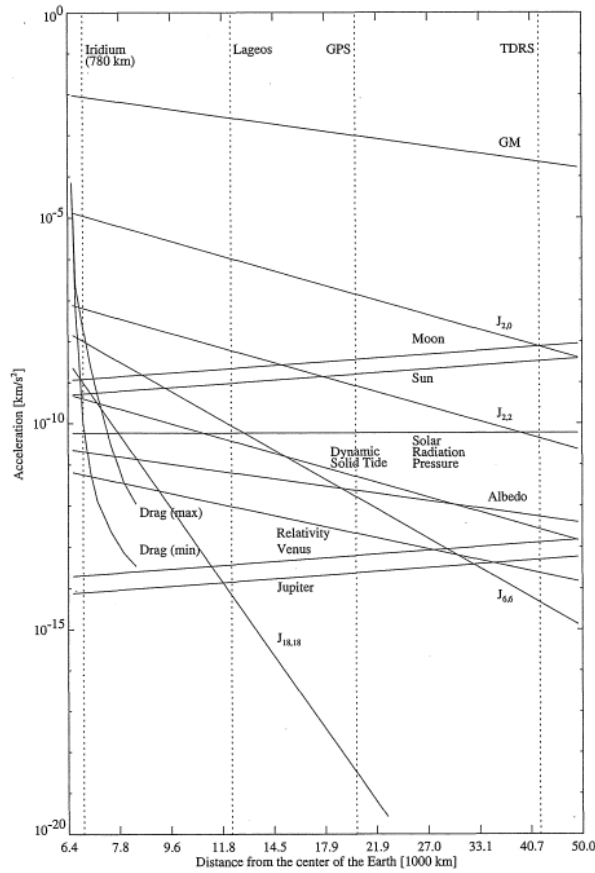


Figure 2.1: Order of magnitude of various perturbations of a satellite's orbit [1]

altitude). Hence orbit control in terms of orbit maintenance and stationkeeping, where the satellite is controlled to be located within a predefined box on a given orbit, is crucial for every space mission that shall last for more than those few years. Additionally, orbit control is also necessary for satellite rendezvous (like the docking of the ATV (Automated Transfer Vehicle) with the ISS (International Space Station)) and for the maintenance of relative orientations in formation flying. For the orbit control of a satellite, it is essential to know the satellite's position and velocity in order to be able to compute the necessary control thrusts. The process of finding the satellite's position and velocity is called orbit determination. [2]

Several options exist for carrying out the orbit determination, which differ in accuracy, operating range and of course in the underlying measurement tech-

nique. Additionally the different methods can be categorized in autonomous, non-autonomous and semi-autonomous systems. An autonomous orbit determination system is for example the combined Earth-/Star-Sensor, that uses the direction and distance to Earth given by the Earth-Sensor as well as the attitude determined by the Star-Sensor in order to calculate the position and velocity of the satellite [26]. This technique can be used from LEO to GEO (Geostationary Earth Orbit) and needs no support from ground or other external sources. A non-autonomous orbit determination system is for example the ground tracking, that uses range and range rate measurements obtained by for example radar tracking by a ground station to calculate the satellite's position and velocity [2]. This technique can as well be used from LEO to GEO and the support from ground is an essential prerequisite for this method. The GPS (Global Positioning System, more explanation below) is an example for a semi-autonomous orbit determination system, that basically uses range and range rate of four different GPS satellites to determine the position and velocity of the satellite. This technique can also be used in LEO as well as in GEO [27]. The GPS is called semi-autonomous due to the fact it basically calculates the position and velocity of the satellite independently but requires a functional GPS satellite network in order to do so. The GPS is a precise orbit determination system that performs in real-time. It will be discussed in detail in the next chapter.

## 2.2 GNSS receivers

A Global Navigation Satellite System (GNSS) is a system of satellites that provides global positioning for GNSS receivers. In this work, the NAVSTAR GPS (NAVigation System with Time and Ranging Global Positioning System), from now on referred to as GPS, will be discussed in detail representatively for all GNSS.

The GPS constellation comprises 24 satellites deployed in six evenly spaced planes, four satellites per plane, with an inclination of  $55^\circ$  and moving in a near-circular orbit with an altitude of 20 200 km, therewith providing a continuous and global coverage.

The GPS satellites transmit carrier signals at the L1 frequency (1575.42 MHz)

and L2 frequency (1227.60 MHz), both having binary codes modulated onto them. The first binary code is the Coarse Acquisition (C/A) code that is modulated on the L1 carrier and publicly available. The Precise (P) code is modulated both on the L1 and L2 carrier phases and is the basis for military use, i.e. when having enabled a certain Anti-Spoofing (AS) mode, the P code is encrypted into a Y code that requires a classified AS module with cryptographic keys. The C/A - and P codes are pseudorandom noise (PRN) codes and each GPS satellite has its own specific and different PRN, thus the GPS satellites may uniquely be identified through the PRN number. The third binary code comprises the navigation data and is added to the C/A and P(Y) codes. The navigation data contains low- and high-accuracy GPS satellites orbit data, as well as clock corrections and other information including but not limited to the Klobuchar parameters used for terrestrial ionospheric corrections (see chapter 4.1 for more details).

For each signal received from a specific GPS satellite, the GPS receiver calculates a so-called pseudorange,  $\rho$ , by comparing the received GPS satellite code with a replica code generated in the receiver. Here, the replica code is shifted in time until the cross-correlation of the two codes reaches a maximum. The resulting code phase yields to the reception time at the receiver clock,  $t_r$ . The signal transmission time,  $t_t$ , is obtained from the received GPS satellite code, thus yielding the pseudorange

$$\rho = c \cdot (t_r - t_t) \quad (2.2.1)$$

with  $c$  being the speed of light. Due to the fact that the receiver and GPS satellite clock do not perfectly match GPS time, the reception and transmission time are expressed in GPS time plus clock bias from GPS time, thus giving

$$\rho = c \cdot [(t_r^{GPS} + \delta t_r) - (t_t^{GPS} + \delta t_t)] \quad (2.2.2)$$

with  $t_r^{GPS}$  and  $t_t^{GPS}$  being the reception and transmission time, respectively, expressed in GPS time and  $\delta t_r$  and  $\delta t_t$  the receiver and GPS satellite clock bias from GPS time, respectively. Re-arranging and using  $\Delta t^{GPS} = t_r^{GPS} - t_t^{GPS}$  yields to

$$\rho = c \cdot (\Delta t^{GPS} + \delta t_r - \delta t_t) \quad (2.2.3)$$

The signal travel time  $\Delta t^{GPS}$  from GPS satellite to receiver is additionally depen-

dent on several factors including but not limited to tropospheric - and ionospheric refraction as well as multipath effects. Through expressing the signal travel time by the time that a completely undisturbed signal would need,  $t_u$ , and the aforementioned errors,  $\Delta_t$ , it follows

$$\rho = c \cdot [(t_u + \Delta_t) + \delta t_r - \delta t_t] \quad (2.2.4)$$

The geometrical distance from GPS satellite to receiver is now simply given by  $\rho_g = c \cdot t_u$  and with  $\Delta = c \cdot \Delta_t$  one obtains

$$\rho = \rho_g + \Delta + c \cdot (\delta t_r - \delta t_t) \quad (2.2.5)$$

The GPS satellite clock bias,  $\delta t_t$ , can be determined with the information provided in the navigation message, hence it will be considered as known from now on and set to zero without loss of generality. For the geometrical distance it applies  $\rho_g = \sqrt{(x_t - x_r)^2 + (y_t - y_r)^2 + (z_t - z_r)^2}$ , with  $(x_t, y_t, z_t)$  being the three-dimensional position of the GPS satellite and  $(x_r, y_r, z_r)$  the three-dimensional position of the receiver, thus giving

$$\rho = \sqrt{(x_t - x_r)^2 + (y_t - y_r)^2 + (z_t - z_r)^2} + \Delta + c \cdot \delta t_r \quad (2.2.6)$$

The position of the GPS satellite can be determined with the information provided in the navigation message again, thus the remaining four unknowns of the system,  $x_r, y_r, z_r$  and  $\delta t_r$  (neglecting  $\Delta$  for the moment), i.e. the position of the receiver and the receiver clock bias, can be determined by combining the pseudoranges from four different GPS satellites. [1]

In reality, the error sources causing the path delay  $\Delta$  can of course not be neglected, hence the different errors have to be accounted for by either directly calculating or modeling them. The biggest error source of  $\Delta$  is ionospheric refraction that causes path delays of up to several 100 m. Hence, the accuracy of the calculated receiver position depends highly on the correction of those ionospheric effects. The following chapter will give details on the ionospheric refraction as last part of the background information, before in chapter 3 and following the treatment of the ionospheric error is discussed in detail.

## 2.3 The Ionosphere and its influence on GNSS receivers

The ionosphere is the upper part of the atmosphere that reaches from an altitude of approximately 50 km up to 1000 km. The name "ionosphere" comes from the fact that this part of the atmosphere is ionized, primarily due to the absorption of solar ultraviolet radiation. Due to the fact that above 50 km altitude the atmosphere gets thin enough for the electrons to exist freely next to the positive ions, the ionosphere contains a plasma. The degree of ionization is measured in terms of electron (or plasma -) density, which is about  $10^8$  electrons/m<sup>3</sup> at 50 km altitude, increasing with height due to the increasing intensity of solar radiation and goes up to  $10^{12}$  electrons/m<sup>3</sup> (for times of high solar activity, thus high solar radiation) at approximately 300 km. Above 300 km, the electron density decreases again due to the fact that the atmospheric density decreases. The ionosphere can be divided into to D region (60-90 km), E region (105-160 km), F1 region (160-180 km) and F2 region (200-1000 km). At night, the F2 region remains the only significantly ionized part of the ionosphere and also the maximum electron density in the ionosphere can be found in the F2 region at about 300 km.

The electron density is highly variable and mainly depends on middle- and long-term solar activity, short-scale solar events like solar flares and day and night variations as well as altitude variation. Figure 2.2 shows how the electron density changes with altitude as well as with day/night cycle and solar activity.

The above mentioned day/night variation results from the solar ultraviolet radiation that produces a variation of the atmospheric density through heating. The solar activity variation comprises a middle-term 27-day period which is related to the rotation period of the Sun and a long-term 11-year period given by the Sun spot cycle. Both these variations have effects on the ionosphere through the extreme ultraviolet radiation of the Sun, which was found to be related to variations in the solar 10.7 cm flux,  $F_{10.7}$ . Hence, the variation of the solar 10.7 cm flux can directly be related to the electron density. As an example, the  $F_{10.7}$  variation due to the long-term 11-year Sun spot cycle is shown in figure 2.3. Without going into further details concerning the high and manifold electron density variability,

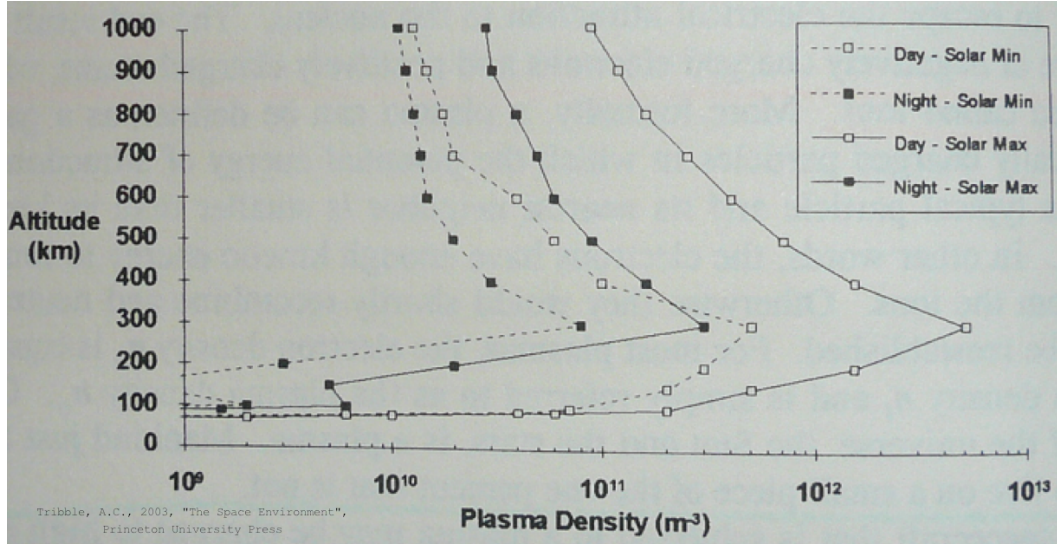


Figure 2.2: Altitude vs. electron density for day/night - and solar activity variation [17]

it can easily be seen that modeling of the electron density is extremely difficult.

Electromagnetic waves like the GPS signals that pass the ionosphere during their way from GPS satellite to receiver, interact with the electrons and ions of the ionosphere's plasma. Hereby, due to a change in electron density, a change of the refractive index is caused that translates into a time - and thus path delay of the signal.

Under the assumption that perturbations due to ions, Earth's magnetic field and absorption effects are neglected, the ionospheric group refractive index,  $n_{gr}$ , is given as

$$n_{gr} = \sqrt{1 + \frac{f_p^2}{f^2}} \approx 1 + \frac{1}{2} \frac{f_p^2}{f^2} \quad (2.3.1)$$

with  $f$  being the frequency of the signals and  $f_p = \frac{1}{2\pi} \sqrt{\frac{d_e e_0^2}{m_e \epsilon_0}}$  the plasma frequency, where  $d_e$  is the electron number density,  $e_0$  the electron charge,  $m_e$  the electron mass and  $\epsilon_0$  the vacuum dielectric constant.

The path delay due to the change of ionospheric group refractive index for a

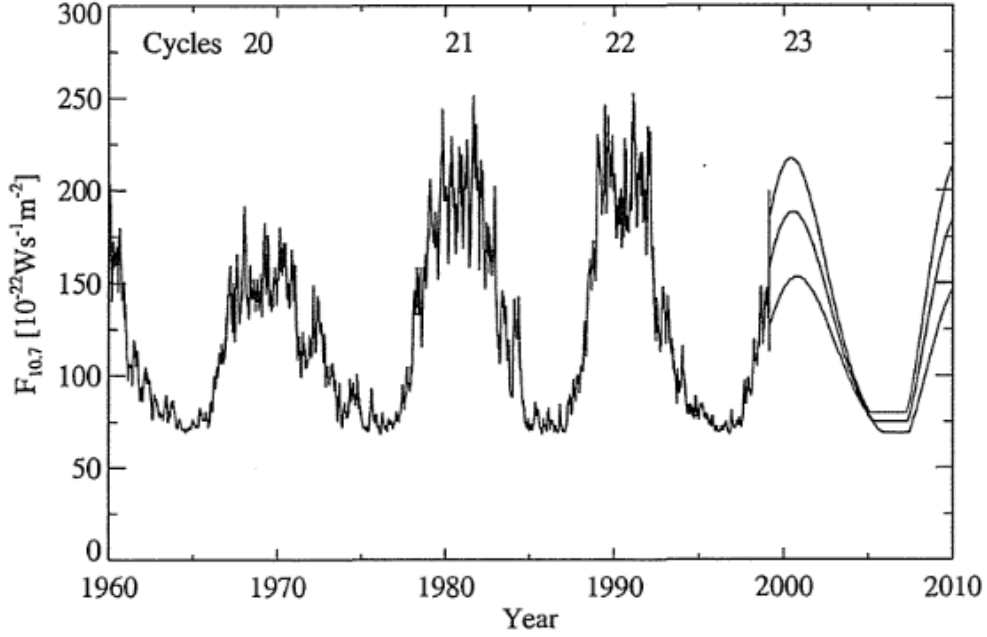


Figure 2.3: "Monthly averages of the solar flux for solar cycles 20-23." [1]

signal propagating from GPS satellite  $S$  to the receiver  $R$  is given as

$$\Delta\rho = \int_S^R (n_{gr} - 1) ds \quad (2.3.2)$$

By substituting  $n_{gr}$  with equation (2.3.1) and inserting the values for  $e_0$ ,  $m_e$  and  $\epsilon_0$ , it directly follows

$$\Delta\rho = \frac{40.3}{f^2} \left[ \frac{m^3}{s^2} \right] TEC \quad (2.3.3)$$

with  $TEC = \int_S^R d_e ds$  being the slant total electron content, i.e. the electron number density,  $d_e$ , integrated along the path  $s$  from GPS satellite  $S$  to receiver  $R$ . A commonly used unit when dealing with ionospheric effects is the TEC unit (TECU) whereby 1 TECU corresponds to an electron column density of  $10^{16} \text{ m}^{-2}$ . [1]

It can be seen that the ionospheric path delay  $\Delta\rho$ , which is the main contributor to the error  $\Delta$  in equation (2.2.6), is directly dependent on the total electron content  $TEC$  and thus on the electron density  $d_e$ . As mentioned above, the electron

density is highly variable and hardly predictable, making the ionospheric path delay hardly predictable as well. Due to the fact that ionospheric refraction can cause path delays of up to several 100 m, it is extremely important for precise positioning and thus precise orbit determination to find models and algorithms to correct for this ionospheric error. Providing such correction models and algorithms is the task of this Master thesis and will be dealt with in detail in the next chapters.

# Requirement analysis and -specification

## 3.1 Functional requirements

The accuracy of Astrium's MosaicGNSS receiver shall be increased from currently 10 m rms (root mean square) 3D position error (in LEO) [3] to the best possible value by implementing new models or algorithms for ionospheric corrections into the navigation module. The ionospheric models are supposed to be applicable to spaceborne GNSS receivers and the algorithms shall be based on single - and double frequency measurements.

A requirement regarding the implementation of the newly developed models and algorithms is that changes in the current MosaicGNSS receiver code are to be minimized. Another issue is that due to computational constraints the number of calculations are to be minimized as well.

In order to test and evaluate the newly implemented models and algorithms, a testing environment shall be set up that is capable of verifying the new implementation by use of simulated and real flight data.

## 3.2 System analysis

### 3.2.1 MosaicGNSS receiver

The MosaicGNSS receiver by EADS Astrium is a fully space qualified 8 channel GNSS receiver that uses a navigation filter to provide a smooth and continuous navigation solution even under restricted GPS visibility [3], [4]. The core of the receiver software comprises three modules, the GPS sensor, the navigation planning and the navigation solution. Due to the fact that the influence of the

ionosphere is handled in the navigation solution, only this module is analyzed in detail. Possible changes in the other two modules are discussed and analyzed in detail when they arise. A detailed description of the MosaicGNSS receiver's navigation algorithms can be found in [4].

The navigation solution module mainly consists of a kinematic solution, which gives an instantaneous navigation solution with 4 or more satellites in track, and a dynamic solution that uses a Kalman filter to determine the navigation solution and needs at least 2 visible satellites. The frequency with which both methods provide a navigation solution is given by 1 Hz.

Both the kinematic - and dynamic solution account for ionospheric effects in the received GPS signal by subtracting a ionospheric correction term from the pseudorange measurement. The currently implemented model for ionospheric corrections is the "Lear ionospheric model" [5] with a TEC (Total Electron Content) value that is dependent only on the position of the Sun and the spacecraft (S/C) position. The formulas for this ionospheric correction can be found in [4, ch. 2.4.3.2].

### **3.2.2 Testing environment**

In order to evaluate the navigation module of the MosaicGNSS receiver, a software simulation environment based on Matlab/Simulink [6] is available as well as the possibility to test the real hardware with a Spirent GNSS Constellation Simulator [7].

The software simulation environment based on Matlab/Simulink (from now on called S/W simulator) has been developed for performance evaluation of on-board orbit determination by GNSS and was itself evaluated by comparison to a real-time test-environment. This analysis focusses on the simulation of the ionospheric delay error, a detailed design description of the whole S/W simulator can be found in [6].

According to the realization of ionospheric correction in the Mosaic GNSS receiver, the ionospheric delay is introduced in the S/W simulator by adding an ionospheric correction term to the simulated pseudorange. The currently imple-

mented model for the ionospheric delay error is the "Lear ionospheric model" with a TEC (Total Electron Content) value that is dependent only on the position of the Sun and the spacecraft position. The formulas for this ionospheric delay error can be found in [6, ch. 4.2.6].

In order to make a difference between the simulated ionospheric delay error and the ionospheric correction (both are basically using the same algorithms), the TEC value in the navigation module is set to a fraction of the TEC value originally used in the simulation to calculate the ionospheric delay on the pseudorange.

The hardware simulation based on the Spirent GNSS Constellation Simulator (from now on called Spirent) can be used to test the real hardware, i.e. the MosaicGNSS receiver, with simulated GPS signals as they would be send from the GPS satellites [7], [8].

The model used by the Spirent to simulate the ionospheric delay is basically also given by either the "Lear ionospheric model" for space applications, where a constant TEC model or a polynomial TEC model can be used, or the Klobuchar model [9] for terrestrial applications. A detailed description of these ionospheric models, their parameters and the Spirent's software in general can be found in [8].

## **3.3 Functional specification**

### **3.3.1 MosaicGNSS receiver**

The ionospheric delay error is dependent on the frequency of the transmitted signal. By combining measurements from signals with two different frequencies, the ionospheric delay error can be reduced by 99 % [10]. Due to the fact that the MosaicGNSS receiver is a single-frequency receiver only, no dual-frequency algorithms can be applied here, thus ruling out the possibility of the best possible reduction of the ionospheric delay error. Nevertheless, due to the fact the Lion Navigator, the successor of the MosaicGNSS receiver [11], will be able to perform dual-frequency-measurements, such a dual-frequency algorithm for a 99 % ionospheric correction will be developed after all.

Feasible ionospheric correction algorithms for single-frequency receivers are the GRAPHIC (Group and Phase Ionospheric Calibration) code and more general, the DRVID (Differenced Range versus Integrated Doppler) technique, that make use of a ionospheric-free (99 %) combination of C/A code and L1 phase observations [12, 18]. In order to stick to the requirement of changing as little code as possible, the navigation filter of the MosaicGNSS receiver itself is not being changed, but the GRAPHIC code / DRVID technique will be used to determine again the ionospheric delay error, which is then subtracted from the pseudorange measurement.

The "Lear ionospheric model" that is implemented in the current navigation solution of the MosaicGNSS receiver, is based on a TEC value that is dependent only on the position of the Sun and the spacecraft. A first step of increasing the accuracy of the ionospheric correction is to change the determination of the TEC value to a more realistic, model-based estimate. Thus, the Klobuchar model, formally known as the Ionospheric Correction Algorithm (ICA), will be implemented that calculates the TEC value for a given latitude, longitude, elevation, azimuth and time. The parameters needed for the Klobuchar model are included in the GPS message and can thus directly be used in the navigation solution. The Klobuchar model is the standard model for terrestrial ionospheric corrections for single-frequency receivers and corrects the pseudorange for about 50 % of the ionospheric delay error [10]. It will be adapted for S/C use by applying a geometrical mapping function that accounts for the elevation dependency of the path length through the ionosphere on a LEO orbit [5].

An other model for ionospheric correction of single-frequency measurements that will be implemented is the "Montenbruck model" [13]. This model uses a thin layer approximation and calculates the ionospheric delay error by using the Klobuchar model and a mapping function, which accounts for the elevation dependency of the path length through the ionosphere, for obtaining the vertical and slant TEC value, respectively. Additionally, a scaling factor is applied by assuming a Chapman profile for the altitude variation of the electron density. Montenbruck & Gill [13] achieved by use of this model for their test case based on single-frequency measurements a 90 % correction of the ionospheric delay error.

Summarizing it can be said, that ionospheric corrections for single-frequency applications based on the following methods will be implemented:

- "Lear ionospheric model", based on TEC values by the Klobuchar model and an elevation-dependent mapping function
- "Montenbruck model", based on TEC values by the Klobuchar model, an elevation-dependent mapping function and an altitude-dependent scaling factor
- GRAPHIC code / DRVID technique (99 % ionospheric correction)

Additionally, a dual-frequency algorithm will be implemented that provides a ionospheric correction of 99 % by combining the pseudoranges from two signals with different frequencies.

### 3.3.2 Testing environment

The S/W simulator and the Spirent have the big disadvantage that they produce the ionospheric delay errors by use of models. For double-frequency applications this doesn't matter due to the fact that the ionospheric delay errors are reduced by 99 % independently of the magnitude of the error [10]. But for single-frequency applications (not considering the GRAPHIC code / DRVID technique), where the ionospheric delay error is reduced by use of models that try to resemble reality, it strongly matters if the produced errors arise from any models or are given by reality. Hence, correcting an ionospheric delay error by use of the same model with which the error has been produced could yield misleadingly good results.

As a consequence, to be able to make reasonable predictions about the quality of the newly implemented algorithms for ionospheric correction, measurement data from real space missions (that also contain the real ionospheric delay) shall be used. The resulting navigation solution shall then be compared with the solution given by tracking the S/C from ground via laser ranging for example or by comparison with the navigation solution given by dual-frequency measurements, where the ionospheric delay error was reduced by 99 %.

The implementation of real measurement data is done in the S/W simulator by bypassing the simulation part and directly giving the real measurements, which

have been previously recorded and converted into a Matlab file, as input to the navigation module. Additionally, for evaluating the GRAPHIC - and the double-frequency code, the S/W simulator is adapted to be able to process carrier phase - and double-frequency measurements, respectively. Furthermore, for testing the Klobuchar model, the S/W simulator has to be able to process the Klobuchar parameters as well.

# System design and - specification

## 4.1 Klobuchar model

As described in chapter 3.3, the Klobuchar model is the standard model for terrestrial ionospheric corrections for single-frequency receivers. The derivation of the model can be found in [9], the algorithm that was used in this work, i.e. an implementation of the Klobuchar model for GPS, comes from the GPS Interface Specification document [16]. With this model, the time delay of the GNSS signal due to ionospheric effects,  $\Delta T_{\text{iono}}$  (in [s]), can be estimated by

$$\Delta T_{\text{iono}} = \begin{cases} F \cdot \left[ 5 \cdot 10^{-9} + (AMP) \cdot \left( 1 - \frac{x^2}{2} + \frac{x^4}{24} \right) \right] & , \text{ if } |x| < 1.57 \\ F \cdot [5 \cdot 10^{-9}] & , \text{ if } |x| \geq 1.57 \end{cases} \quad (4.1.1)$$

with  $F$  being the slant factor,  $AMP$  (in [s]) the amplitude and  $x$  (in [rad]) the phase of the cosine representation of the diurnal vTEC variation. Those values are calculated via

$$F = 1 + 16 \cdot [0.53 - E]^3 \quad (4.1.2)$$

$$AMP = \begin{cases} \sum_{n=0}^3 \alpha_n \cdot \phi_m^n & , \text{ if } AMP \geq 0 \\ 0 & , \text{ if } AMP < 0 \end{cases} \quad (4.1.3)$$

$$x = \frac{2\pi (t - 50400)}{PER} \quad (4.1.4)$$

with  $E$  being the elevation angle between user and satellite (in [semi-circles]),  $\phi_m$  the geomagnetic latitude of the Earth projection of the ionosphere intersection point (mean ionospheric height assumed to be 350 km) (in [semi-circles]),  $\alpha_n$  ( $n = 0, 1, 2, 3$ ) the first 4 Klobuchar parameters that are broadcasted in the GPS navigation message (in [s], [s/semi-circles], [s/semi-circles<sup>2</sup>] and [s/semi-circles<sup>3</sup>], respectively),  $t$  the local time (in [s]) and  $PER$  (in [s]) the period of the

cosine representation of the diurnal vTEC variation, which is given as

$$PER = \begin{cases} \sum_{n=0}^3 \beta_n \cdot \phi_m^n & , \text{ if } PER \geq 72,000 \\ 72,000 & , \text{ if } PER < 72,000 \end{cases} \quad (4.1.5)$$

with  $\beta_n$  ( $n = 0, 1, 2, 3$ ) the other 4 Klobuchar parameters that are broadcasted in the GPS navigation message (in [s], [s/semi-circles], [s/semi-circles<sup>2</sup>] and [s/semi-circles<sup>3</sup>], respectively).

The geomagnetic latitude  $\phi_m$  (in [semi-circles]) is calculated by

$$\phi_m = \phi_i + 0.064 \cdot \cos(\lambda_i - 1.617) \quad (4.1.6)$$

with  $\phi_i$  and  $\lambda_i$  being the geodetic latitude and longitude of the Earth projection of the ionospheric intersection point (in [semi-circles]), respectively. These values are calculated via

$$\phi_i = \begin{cases} \phi_u + \psi \cdot \cos(A) & , \text{ if } |\phi_i| \leq 0.416 \\ +0.416 & , \text{ if } \phi_i > +0.416 \\ -0.416 & , \text{ if } \phi_i < +0.416 \end{cases} \quad (4.1.7)$$

$$\lambda_i = \lambda_u + \frac{\psi \cdot \sin(A)}{\cos(\phi_i)} \quad (4.1.8)$$

with  $\phi_u$  and  $\lambda_u$  being the user geodetic latitude and longitude (in [semi-circles], WSG-84), respectively,  $A$  the azimuth angle between user and satellite, measured clockwise positive from true North (in [semi-circles]) and  $\psi$  the Earth's central angle between user position and Earth projection of ionospheric intersection point (in [semi-circles]), which is determined by

$$\psi = \frac{0.0137}{E + 0.11} - 0.022 \quad (4.1.9)$$

Finally, the local time  $t$  (in [s]) is determined by help of the GPS time  $t_{GPS}$  (in [s]) via

$$t = \begin{cases} 4.32 \cdot 10^4 \cdot \lambda_i + t_{GPS} & , \text{ if } 0 \leq t < 86,400 \\ 4.32 \cdot 10^4 \cdot \lambda_i + t_{GPS} - 86,400 & , \text{ if } t \geq 86,400 \\ 4.32 \cdot 10^4 \cdot \lambda_i + t_{GPS} + 86,400 & , \text{ if } t < 0 \end{cases} \quad (4.1.10)$$

The ionospheric path delay,  $\Delta\rho_{\text{iono,K}}$  (in [m]), can thus be calculated via

$$\Delta\rho_{\text{iono,K}} = \Delta T_{\text{iono}} \cdot c \quad (4.1.11)$$

with  $c$  being the speed of light and  $\Delta T_{\text{iono}}$  the ionospheric time delay from equation (4.1.1).

With this model, a correction of the ionospheric delay error of about 50 % can be achieved. Due to the fact that the Klobuchar model is meant to be used for terrestrial applications only, it has to be adapted for use in space, what is shown in the next chapters in two different ways.

## 4.2 Lear & Lear/Klobuchar model

The Lear model is the currently implemented model for ionospheric corrections in the navigation solution of the MosaicGNSS receiver [4]. It was developed by W.M. Lear and is described in detail in [5].

In general, the ionospheric path delay for L1 frequency observations,  $\Delta\rho_{\text{iono}}$  (in [m]) is given by [1]

$$\Delta\rho_{\text{iono,L}} = \frac{40.3}{f_{L1}^2} \left[ \frac{m^3}{s^2} \right] \cdot TEC \quad (4.2.1)$$

with  $f_{L1} = 1575.42$  MHz being the L1 frequency and  $TEC = \int Ndl$  the slant total electron content, i.e. the electron number density,  $N$ , integrated along the path from user to GPS satellite.

The Lear model makes use of an elevation dependent geometrical mapping function,  $m(E)$ , to map the vertical TEC,  $vTEC$ , to the slant TEC by assuming the electron density to be described by a Chapman profile with scale height of 75 km

and a height of maximum electron density of 300 km. This yields to

$$TEC = vTEC \cdot m(E) = vTEC \cdot \frac{2.037}{\sqrt{\sin^2 E + 0.076} + \sin E} \quad (4.2.2)$$

with  $E$  being the elevation angle measured relative to the local horizon plane at the location of the user.

Additionally, a position dependent vertical TEC variation is assumed, where the vertical TEC varies with position of user and Sun. The amplitude of this variation is set to 14.3 % of a reference value,  $vTEC_0$ , giving

$$vTEC = (1 + 0.143 \vec{n}_{\text{sun}}^T \cdot \vec{u}_{\text{user}})^8 \cdot \frac{vTEC_0}{TECU} \quad (4.2.3)$$

with  $\vec{n}_{\text{sun}}$  being a unit vector describing the equatorial projection of the Sun direction and  $\vec{u}_{\text{user}}$  a unit vector describing the user direction. The reference vertical TEC,  $vTEC_0$ , is given in TEC units (TECU) whereby 1 TECU corresponds to an electron column density of  $10^{16} \text{ m}^{-2}$ .

Combining those equations, one obtains for the ionospheric path delay for L1 frequency observations,  $\Delta\rho_{\text{iono}}$  (in [m]),

$$\Delta\rho_{\text{iono,L}} = 0.162 \text{ m} \cdot (1 + 0.143 \vec{n}_{\text{sun}}^T \cdot \vec{u}_{\text{user}})^8 \cdot \frac{vTEC_0}{TECU} \cdot \frac{2.037}{\sqrt{\sin^2 E + 0.076} + \sin E} \quad (4.2.4)$$

In order to improve the Lear ionospheric model, the vertical TEC that is in this model only dependent on user position and the position of the Sun will be exchanged by a vertical TEC determined by the Klobuchar model, hence giving a more realistic estimation of the ionospheric error. Combining equations (4.1.11), (4.2.1) and (4.2.2) yields to the ionospheric path delay for L1 frequency observations, estimated by this combination of Lear - and Klobuchar model (later referred to as Lear/Klobuchar model) as follows,

$$\Delta\rho_{\text{iono,L/K}} = \frac{40.3}{f_{L1}^2} \left[ \frac{\text{m}^3}{\text{s}^2} \right] \cdot vTEC \cdot \frac{2.037}{\sqrt{\sin^2 E + 0.076} + \sin E} \quad (4.2.5)$$

$$= \Delta\rho_{\text{iono,K}}|v \cdot \frac{2.037}{\sqrt{\sin^2 E + 0.076} + \sin E} \quad (4.2.6)$$

with  $\Delta\rho_{\text{iono,K}}|v$  being the vertical ionospheric path delay estimated by the Klobuchar model, i.e. the ionospheric path delay  $\Delta\rho_{\text{iono,K}}$  assuming an elevation angle of  $E = \frac{\pi}{2}$  rad and an azimuth angle of  $A = 0$  rad.

### 4.3 Montenbruck model

The "Montenbruck model" as described in [13] uses a thin layer approximation to describe the ionospheric path delay for L1 frequency observations. Here, the residual ionosphere is considered to be concentrated in a single layer at an altitude  $h_{\text{IP}}$  above the user altitude  $h_{\text{S}}$  ( $h_{\text{IP}} > h_{\text{S}}$ ), as can be seen in figure 4.1.

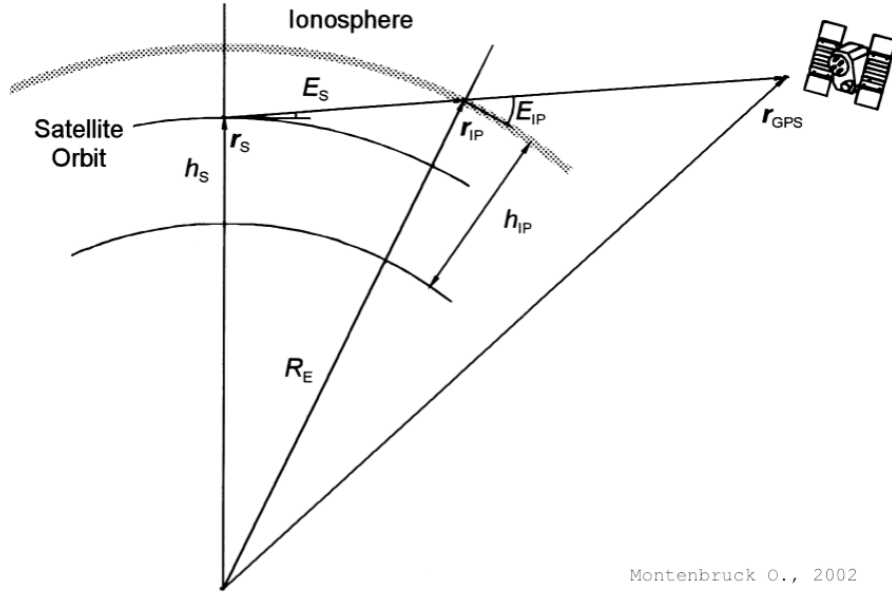


Figure 4.1: Geometry of the Montenbruck model [13]

Starting from the general description of ionospheric path delays (see equation (4.2.1)),

$$\Delta\rho_{\text{iono,M}} = \frac{40.3}{f_{L1}^2} \left[ \frac{m^3}{s^2} \right] \cdot TEC, \quad (4.3.1)$$

the TEC is determined at the ionospheric point  $\vec{r}_{\text{IP}}$ , i.e. the intersection of the line-of-sight between user and GPS satellite and the residual ionospheric layer

(see figure [13]). This TEC is given by

$$TEC = TEC(\vec{r}_{IP}) = \alpha \cdot vTEC \cdot m(E_{IP}) \quad (4.3.2)$$

with  $m(E_{IP}) = \frac{1}{\sin(E_{IP})}$  being the mapping function that was chosen to account for the increase of path length in the ionosphere with decreasing elevation at the ionospheric point,  $E_{IP}$ .

In the same manner than in chapter 4.2, the vertical TEC is calculated by use of the Klobuchar model, i.e.

$$vTEC = \left( \frac{40.3}{f_{L1}^2} \left[ \frac{m^3}{s^2} \right] \right)^{-1} \cdot \Delta\rho_{iono,K}|v \quad (4.3.3)$$

with  $\Delta\rho_{iono,K}|v$  being the vertical ionospheric path delay estimated by the Klobuchar model, i.e. the ionospheric path delay  $\Delta\rho_{iono,K}$  assuming an elevation angle of  $E = \frac{\pi}{2}$  rad and an azimuth angle of  $A = 0$  rad.

The term  $\alpha$  represents a scaling factor that accounts for the altitude variation of the electron density by assuming a Chapman profile with a scale height  $H$  and a height of maximum electron density  $h_0$ . For the geographical coordinates  $(\lambda_{IP}, \phi_{IP})$  of the projection of the ionospheric point to Earth surface, the scaling factor  $\alpha$  relates the TEC of the ionosphere above altitude  $h_{IP}$ ,  $TEC(\lambda_{IP}, \phi_{IP}, h_{IP})$ , to the TEC above ground,  $TEC(\lambda_{IP}, \phi_{IP}, 0)$ , as follows

$$\alpha = \frac{TEC(\lambda_{IP}, \phi_{IP}, h_{IP})}{TEC(\lambda_{IP}, \phi_{IP}, 0)} = \frac{e - \exp(1 - \exp(-z_{IP}))}{e - \exp(1 - \exp(\frac{h_0}{H}))} \quad \text{with } z_{IP} = \frac{h_{IP} - h_0}{H} \quad (4.3.4)$$

This finally yields to the expression for the ionospheric path delay for L1 frequency observations determined by the Montenbruck model,  $\Delta\rho_{iono,M}$  (in [m]),

$$\Delta\rho_{iono,M} = \frac{\alpha}{\sin(E_{IP})} \cdot \Delta\rho_{iono,K}|v \quad (4.3.5)$$

Montenbruck & Gill [13] determined the scaling factor  $\alpha$  in several different ways. It was empirically calibrated by use of dual-frequency measurements, estimated by an adaption of the Chapman profiles to fit to the International Reference

Ionosphere IRI95 density values for the specific days and it was considered as free scaling parameter that was determined by use of a sequential batch filter.

Due to the fact that the MosaicGNSS receiver is a single-frequency receiver, the first option can't be implemented. Requirements of this Master thesis were to minimize changes in the current MosaicGNSS receiver code and to minimize the number of calculations needed to determine the ionospheric error, thus excluding the other two options that have been used by Montenbruck & Gill.

For the implementation of this model, the scaling factor  $\alpha$  will hence be estimated in a post-processing manner (brute-force search) to evaluate the general quality of this model in combination with the MosaicGNSS receiver. If the results show very good performance, the constraints regarding changes in code and computational effort may be lowered and a dynamic filter may be implemented.

## 4.4 GRAPHIC/DRVID

The GRAPHIC (Group and Phase Ionospheric Calibration) code is JPL's implementation of the DRVID (Differenced Range versus Integrated Doppler) technique for satellite orbit determination using single-frequency GPS measurements [18]. It makes use of a ionospheric-free combination of C/A code and L1 phase observations and can thus account for 99% of the ionospheric error [12, 18]. The GRAPHIC code / DRVID technique is adapted to calculate the ionospheric path delay as follows.

The pseudorange based on C/A code measurements,  $\rho_{C/A}$  (in [m]), is given by

$$\rho_{C/A} = \rho_g + \Delta + \Delta\rho_{\text{iono},C/A} + \epsilon_{C/A} \quad (4.4.1)$$

with  $\rho_g$  being the geometrical range,  $\Delta\rho_{\text{iono},C/A}$  the ionospheric path delay on the pseudorange based on C/A code measurements,  $\Delta$  all remaining errors like user clock bias and GPS clock bias and  $\epsilon_{C/A}$  the C/A code measurement noise.

The pseudorange based on L1 phase measurements,  $\rho_{L1P}$  (in [m]), is given by

$$\rho_{L1P} = \lambda_{L1} \cdot \phi_{L1} = \rho_g + \Delta + \Delta\rho_{\text{iono},L1P} + \lambda_{L1} \cdot N + \epsilon_{L1P} \quad (4.4.2)$$

with  $\lambda_{L1}$  being the wavelength of the L1 signal,  $\phi_{L1}$  the (integrated carrier) phase on L1,  $\rho_g$  again the geometrical range,  $\Delta\rho_{\text{iono,L1P}}$  the ionospheric path delay on the pseudorange based on L1 phase measurements,  $\Delta$  all remaining errors like user clock bias and GPS clock bias,  $N$  the integer ambiguity (see [12] for further information) and  $\epsilon_{L1P}$  the L1 phase measurement noise.

By combining the two pseudoranges based on C/A code and L1 phase measurements, it follows

$$\frac{\rho_{C/A} - \rho_{L1P}}{2} = \frac{(\rho_g + \Delta + \Delta\rho_{\text{iono,C/A}} + \epsilon_{C/A}) - (\rho_g + \Delta + \Delta\rho_{\text{iono,L1P}} + \lambda_{L1} \cdot N + \epsilon_{L1P})}{2} \quad (4.4.3)$$

$$= \frac{\Delta\rho_{\text{iono,C/A}} - \Delta\rho_{\text{iono,L1P}} - \lambda_{L1} \cdot N + \epsilon_{C/A} - \epsilon_{L1P}}{2} \quad (4.4.4)$$

Due to the fact that the ionospheric refraction causes the group velocity to decrease and the phase velocity to increase, i.e.  $\Delta\rho_{\text{iono,C/A}} = -\Delta\rho_{\text{iono,L1P}}$ , [1] one obtains

$$\frac{\rho_{C/A} - \rho_{L1P}}{2} = \Delta\rho_{\text{iono,C/A}} - \frac{\lambda_{L1} \cdot N}{2} + \epsilon \quad (4.4.5)$$

with  $\epsilon = \frac{\epsilon_{C/A} - \epsilon_{L1P}}{2}$  being the combined measurement noise.

By derivating equation (4.4.5) and under the assumption that the bias  $b = \lambda_{L1} \cdot N$  is constant over time for each tracked GPS satellite for a continuous track (no cycle slips), i.e.  $\frac{\Delta b}{\Delta t} = 0$ , it follows for the ionospheric path delay

$$\frac{\Delta\rho_{\text{iono,C/A}}}{\Delta t} = \frac{\Delta \left( \frac{\rho_{C/A} - \rho_{L1P}}{2} - \epsilon \right)}{\Delta t} \quad (4.4.6)$$

Hence the change in ionospheric path delay can be accurately calculated without knowledge of the bias  $b$ . Especially it follows

$$\rho_{\text{iono,C/A}}(t) - \rho_{\text{iono,C/A}}(t-1) = \left[ \frac{\rho_{C/A}(t) - \rho_{L1P}(t)}{2} - \epsilon(t) \right] - \left[ \frac{\rho_{C/A}(t-1) - \rho_{L1P}(t-1)}{2} - \epsilon(t-1) \right] \quad (4.4.7)$$

what can be rewritten as

$$\rho_{\text{iono,C/A}}(t) = \frac{\rho_{\text{C/A}}(t) - \rho_{\text{L1P}}(t)}{2} - \frac{\rho_{\text{C/A}}(t-1) - \rho_{\text{L1P}}(t-1)}{2} + \rho_{\text{iono,C/A}}(t-1) - \epsilon_c \quad (4.4.8)$$

with  $\epsilon_c = \epsilon(t) - \epsilon(t-1)$  being the combined measurement noise.

This means that the ionospheric path delay at time  $t$  can be directly calculated with the knowledge of the past ionospheric path delay at time  $t-1$  and the two pseudoranges (from C/A code and L1 phase) at times  $t$  and  $t-1$ .

For the standard deviation  $\sigma$  of the combined measurement noise  $\epsilon_c$  and with the knowledge that  $\sigma(\epsilon(t)) = \sigma(\epsilon(t-1))$  it follows

$$\sigma(\epsilon_c) = \sqrt{\sigma^2(\epsilon(t)) + \sigma^2(\epsilon(t-1))} \quad (4.4.9)$$

$$= \sqrt{2 \cdot \sigma^2 \left( \frac{\epsilon_{\text{C/A}} - \epsilon_{\text{L1P}}}{2} \right)} \quad (4.4.10)$$

$$= \sqrt{2} \cdot \sqrt{\sigma^2 \left( \frac{\epsilon_{\text{C/A}}}{2} \right) + \sigma^2 \left( \frac{\epsilon_{\text{L1P}}}{2} \right)} \quad (4.4.11)$$

Representative standard deviations for the C/A code measurement noise  $\epsilon_{\text{C/A}}$  and for the carrier phase measurement noise  $\epsilon_{\text{L1P}}$  are given by  $\epsilon_{\text{C/A}} = 1$  m and  $\epsilon_{\text{L1P}} = 1$  mm, respectively [12]. The carrier phase measurement noise is thus three orders of magnitudes smaller than the C/A code measurement noise, hence it can be neglected in equation (4.4.11) and it follows

$$\sigma(\epsilon_c) = \sqrt{2} \cdot \sqrt{\sigma^2 \left( \frac{\epsilon_{\text{C/A}}}{2} \right) + \sigma^2 \left( \frac{\epsilon_{\text{L1P}}}{2} \right)} \quad (4.4.12)$$

$$\approx \sqrt{2} \cdot \sqrt{\sigma^2 \left( \frac{\epsilon_{\text{C/A}}}{2} \right)} = \frac{\sqrt{2}}{2} \cdot \sigma(\epsilon_{\text{C/A}}) \quad (4.4.13)$$

Inserting the value of the C/A code measurement noise, one finally obtains a combined measurement noise of  $\sigma(\epsilon_c) \approx 0.7$  m. Hence by combining C/A code and L1 phase observations in the above described manner, the measurement noise is reduced by  $\approx 0.3$  m.

Due to the fact that the GRAPHIC code / DRVID technique, as used in the

way shown above, requires knowledge of the previous C/A code and L1 phase measurements and additionally the previous ionospheric error, a recursive algorithm has to be developed that especially accounts for a proper initialization ( $\rho_{\text{iono,C/A}}(t = 0)$ ). Hence the following algorithm is proposed:

1. Calculate, save and output  $\rho_{\text{iono,C/A}}(t = 0)$  by help of a suitable ionospheric model and save the C/A code and L1 phase measurements  $\rho_{\text{C/A}}(t = 0)$  and  $\rho_{\text{L1P}}(t = 0)$  to memory. Options for the ionospheric model that are analyzed:
  - Lear model
  - Lear/Klobuchar model
  - Montenbruck model
2. Calculate and save  $\rho_{\text{iono,C/A}}(t)$ ,  $t \in \mathbb{N}_{\geq 1}$ , with the previous values  $\rho_{\text{iono,C/A}}(t-1)$ ,  $\rho_{\text{C/A}}(t-1)$  and  $\rho_{\text{L1P}}(t-1)$  and the current values  $\rho_{\text{C/A}}(t)$  and  $\rho_{\text{L1P}}(t)$  by use of equation (4.4.8) and save the C/A code and L1 phase measurements  $\rho_{\text{C/A}}(t)$  and  $\rho_{\text{L1P}}(t)$  to memory.
3. Apply a Low-Pass-Filter of length  $k \in \mathbb{N}$  (best value of  $k$  dependent on measurement time interval) to the ionospheric path delays  $\rho_{\text{iono,C/A}}(\tau)$ ,  $\tau \in \mathbb{N} = [t - k + 1, t]$ ,  $t > k$  and output the result as ionospheric path delay at time  $t$ ,  $\rho_{\text{iono,C/A}}(t)$ .

## 4.5 Dual-frequency correction

As described in chapter 2.3, the ionospheric path delay is frequency-dependent, what can be used to develop a ionospheric-correction by combining two signals with different frequencies. The following derivation is based on the two GPS signals L1 and L2 with  $f_{\text{L1}} = 1575$  MHz,  $f_{\text{L2}} = 1228$  MHz, but it also applies for any other two arbitrary GNSS signals with different frequencies.

The ionospheric path delay on the two signals L1 and L2,  $\Delta\rho_{\text{iono},i}$  (in [m]) with  $i = \{\text{L1}, \text{L2}\}$ , is frequency-dependent and can be described as

$$\Delta\rho_{\text{iono},i} = \frac{40.3}{f_i^2} \left[ \frac{\text{m}^3}{\text{s}^2} \right] \cdot TEC \quad (4.5.1)$$

The pseudorange of the two signals L1 and L2 obtained from code measurements,  $\rho_i$  (in [m]), is given by

$$\rho_i = \rho_g + \Delta + \Delta\rho_{\text{iono},i} + \epsilon_i \quad (4.5.2)$$

with  $\rho_g$  being the geometrical range,  $\Delta$  all (frequency-independent) errors like user clock bias and GPS clock bias,  $\Delta\rho_{\text{iono},i}$  the ionospheric path delay for the signal  $i$  as described above and  $\epsilon_i$  the code measurement noise for  $i$ .

By building the difference of the the two pseudoranges  $\rho_i$ , one obtains

$$\rho_{L2} - \rho_{L1} = \rho_g + \Delta + \Delta\rho_{\text{iono},L2} + \epsilon_{L2} - (\rho_g + \Delta + \Delta\rho_{\text{iono},L1} + \epsilon_{L1}) \quad (4.5.3)$$

$$= \Delta\rho_{\text{iono},L2} - \Delta\rho_{\text{iono},L1} + (\epsilon_{L2} - \epsilon_{L1}) \quad (4.5.4)$$

$$= \frac{40.3}{f_{L2}^2} \left[ \frac{m^3}{s^2} \right] \cdot TEC - \frac{40.3}{f_{L1}^2} \left[ \frac{m^3}{s^2} \right] \cdot TEC + (\epsilon_{L2} - \epsilon_{L1}) \quad (4.5.5)$$

$$= 40.3 \left[ \frac{m^3}{s^2} \right] \cdot TEC \cdot \frac{f_{L1}^2 - f_{L2}^2}{f_{L2}^2 f_{L1}^2} + (\epsilon_{L2} - \epsilon_{L1}) \quad (4.5.6)$$

$$= \frac{40.3}{f_{L1}^2} \left[ \frac{m^3}{s^2} \right] \cdot TEC \cdot \frac{f_{L1}^2 - f_{L2}^2}{f_{L2}^2} + (\epsilon_{L2} - \epsilon_{L1}) \quad (4.5.7)$$

$$= \Delta\rho_{\text{iono},L1} \cdot \frac{f_{L1}^2 - f_{L2}^2}{f_{L2}^2} + (\epsilon_{L2} - \epsilon_{L1}) \quad (4.5.8)$$

By rearranging the previous equation it follows that the ionospheric path delay for the L1 pseudorange obtained from code measurements can be directly calculated via

$$\Delta\rho_{\text{iono},L1} = \frac{f_{L2}^2}{f_{L1}^2 - f_{L2}^2} \cdot (\rho_{L2} - \rho_{L1}) + \epsilon \quad (4.5.9)$$

with the combined code measurement noise  $\epsilon = \frac{f_{L2}^2}{f_{L1}^2 - f_{L2}^2} \cdot (\epsilon_{L1} - \epsilon_{L2})$ .

For the standard deviation  $\sigma$  of the combined code measurement noise  $\epsilon$ , by assuming  $\sigma(\epsilon_{L1}) \approx \sigma(\epsilon_{L2})$ , it follows

$$\sigma(\epsilon) = \sqrt{\sigma^2 \left( \frac{f_{L2}^2 \epsilon_{L1}}{f_{L1}^2 - f_{L2}^2} \right) + \sigma^2 \left( \frac{f_{L2}^2 \epsilon_{L2}}{f_{L1}^2 - f_{L2}^2} \right)} \quad (4.5.10)$$

$$= \frac{f_{L2}^2}{f_{L1}^2 - f_{L2}^2} \sqrt{\sigma^2(\epsilon_{L1}) + \sigma^2(\epsilon_{L2})} \quad (4.5.11)$$

$$\approx \frac{f_{L2}^2}{f_{L1}^2 - f_{L2}^2} \sqrt{2} \cdot \sigma(\epsilon_{L1}) \quad (4.5.12)$$

Inserting the values for  $f_{L1}$  and  $f_{L2}$ , one obtains

$$\sigma(\epsilon) \approx 2.2 \cdot \sigma(\epsilon_{L1}) \quad (4.5.13)$$

A representative standard deviation for the C/A code measurement noise  $\epsilon_{L1}$  is [12]  $\sigma(\epsilon_{L1}) = 1$  m, thus yielding to an error of  $\sigma(\epsilon) \approx 2.2$  m. Hence, the calculation of the ionospheric path delay for the L1 pseudorange by use of a combination of the two pseudoranges from signals L1 and L2 yields to an additional noise of  $\approx 2.2$  m in the system.

Here it is important to mention that this additional code measurement noise is usually white gaussian noise, what can efficiently be removed by use of a Kalman filter, for example. The (non-gaussian) error due to ionospheric effects on the other hand, which can be treated poorly with Kalman filters, is strongly reduced, thus yielding to a highly increased accuracy in S/C position and -velocity.

## 4.6 Data editing

In order to remove outliers due to invalid or degraded measurements from the data sets, four data editing criteria are applied as follows.

Firstly, only GPS SVs with elevation angles of more than  $10^\circ$  are considered as valid input for the navigation module. This is due to the fact that signals at elevations of less than  $10^\circ$  significantly contribute to the overall ionospheric error budget just because their geometrical path through the ionosphere is longer and thus their TEC higher.

Secondly, the change of ionospheric path delay is restricted to be less than 200 m/s. This single-frequency data editing criteria is based on C/A code pseudoranges and L1 phase measurements and compares those two measurements from two time epochs by use of equation (4.4.6) in order to obtain the change in iono-

spheric error. If the change in ionospheric path delay is bigger than 200 m per second, then either a huge solar event like a huge solar flare has taken place or the measurement at this time is invalid or degraded. In both ways, this measurement should be excluded from the navigation solution.

The third data editing criteria concerns the residuals of the pseudorange differences of measurement and model. Here, if at least 2 satellites (compared to another reference satellite) are available with residuals smaller than 50 m, then all other GPS SVs with residuals bigger than 50 m are excluded from the navigation solution.

Fourthly, the GPS SVs with less than 35 dB Hz carrier-to-noise density ( $C/N_0$ ) are also excluded from the navigation solution. This is due to the fact that signals with less than 35 dB Hz  $C/N_0$  have a higher probability of being degraded. Furthermore, the measurement noise increases with decreasing  $C/N_0$ .

## 4.7 Summary

The ionospheric corrections as described in detail in the previous chapters are implemented and evaluated in the following combinations:

- Lear model (currently used model in the MosaicGNSS receiver)
- Lear/Klobuchar model
- Montenbruck model
- DRVID + Lear model
- DRVID + Lear/Klobuchar model
- DRVID + Montenbruck model
- Double frequency correction

Additionally, four data editing criteria are implemented in order to remove outliers due to invalid or degraded measurements from the data sets.

# Implementation and testing

## 5.1 MosaicGNSS receiver

The ionospheric corrections as described in chapter 4 are implemented in the MosaicGNSS receiver navigation solution module as autonomous functions, written in C, that can be independently integrated in the current flight code by just changing one function call. Due to the computational constraints as described in chapter 3.1, during implementation attention was drawn to efficiency and simultaneously to ease of code readability.

## 5.2 CHAMP mission

In order to be able to make reasonable predictions about the quality of the newly implemented algorithms for ionospheric correction, measurement data from a real space mission is used. The selected real space mission is the Challenging Minisatellite Payload (CHAMP) mission, a german small satellite mission under the lead of the GeoForschungsZentrum (GFZ) Potsdam. CHAMP was launched on July 15th, 2000 into a near-circular, near-polar low Earth orbit (LEO) with an initial altitude of 454 km [19].

CHAMP is equipped with a Blackjack GPS receiver developed by the Jet Propulsion Laboratory (JPL). The Blackjack GPS receiver processes code and phase measurements on both the L1 and L2 frequency and provides those measurements for typically 10 satellites simultaneously [24].

The CHAMP measurement data is provided in the Rinex format for GPS observation data plus some CHAMP-specific adaptations [21, 22] and comprises the observables L1 (phase measurement on C/A channel), L2 (phase measurement on L2), C1 (C/A code), P1 (P-code on L1), P2 (P-code on L2), S1 (SNR on L1), S2 (SNR on L2), LP1 (phase measurement on L1) and SA (SNR for C/A channel).

The reference orbit is given by the Rapid Science Orbits (RSO) of the CHAMP Information System and Data Center (ISDC) [20]. The data is given in the CHAMP orbit format [23] and has a 3D position error RMS of 5 cm.

The data of the navigation message, i.e. Almanac, Ephemerides and IONO/UTC message, is obtained from the International GNSS Service (IGS). Here, the navigation messages of the particular dates can be downloaded as they have been originally broadcasted during that time. The navigation message data is given in the Rinex format for GPS navigation messages [21].

### 5.3 Matlab/Simulink environment

A testing environment is set up that is based on the already existing Matlab/Simulink software simulator (from now on called S/W simulator) as described in chapter 3.2.2.

The possibility of feeding the navigation module with real flight data instead of simulated data is realized by completely bypassing the simulation part and directly giving the real measurements, which have been previously recorded and converted into a Matlab file, as input to the navigation module. The real flight data from CHAMP (see chapter 5.2), which is provided in the Rinex format for GPS observation data plus some CHAMP-specific adaptations [21, 22], is imported and converted into the data structure needed by the S/W simulator. Additionally, an algorithm is developed to reduce the number of tracked satellites from  $\approx 10$  in the CHAMP data to 8 in order to fit to the 8-channel structure of the MosaicGNSS receiver.

The data of the navigation message, comprising Almanac, Ephemerides and IONO/UTC message, that also comes from an external source (IGS, see chapter 5.2) is given in the Rinex format for GPS navigation messages [21] and imported and converted into the data structure needed by the S/W simulator.

In order to compare the calculated navigation solution with a reference, the CHAMP rapid science orbit data (see chapter 5.2), which is given in the CHAMP orbit format [23], is as well imported and converted into the data structure needed

by the S/W simulator.

Additionally, for evaluating the GRAPHIC code / DRVID technique and the double-frequency correction, the S/W simulator is adapted to be able to process carrier phase - and double-frequency measurements, respectively. Furthermore, for testing the Klobuchar model, the S/W simulator is adapted to process the Klobuchar parameters as well.

For comparison between the ionospheric error calculated by the navigation solution and the reference ionospheric error, an evaluation tool is developed that analyzes different aspects like  $C/N_0$ , elevation angle etc. of the signals for which the ionospheric errors were calculated. The reference ionospheric error here is calculated by use of P1 and P2 pseudorange measurements via equation (4.5.9).

## 5.4 Testing

During the implementation phase, every completed part of an algorithm is extensively tested. Functional tests are performed for the completed algorithms as well as plausibility tests. Finally, the different combinations of algorithms (like DRVID + Montenbruck model) are tested and verified.

# Evaluation

## 6.1 Selected GPS data sets

In total 4 data sets of the CHAMP GPS data have been selected. The selection was based on the concern to cover a preferably large range of different ionospheric conditions. As can be seen in figure 6.1, the solar 10.7 cm radio flux, which is an indicator for the sun activity and thus the ionospheric path delay (see chapter 2.3), reached a maximum in beginning 2002 and has decreased since then to a minimum value in 2008/2009. Thus, 4 data sets have been selected that were recorded on days with decreasing sun activity, i.e. 15. January 2002 (day of year (DOY) 15, 24h data arc at 10 s steps), 7. August 2003 (DOY 219, 24h data arc at 10 s steps), 7. August 2004 (DOY 220, 19.5h data arc at 10 s steps) and 10. November 2008 (DOY 315, 24h data arc at 10 s steps).

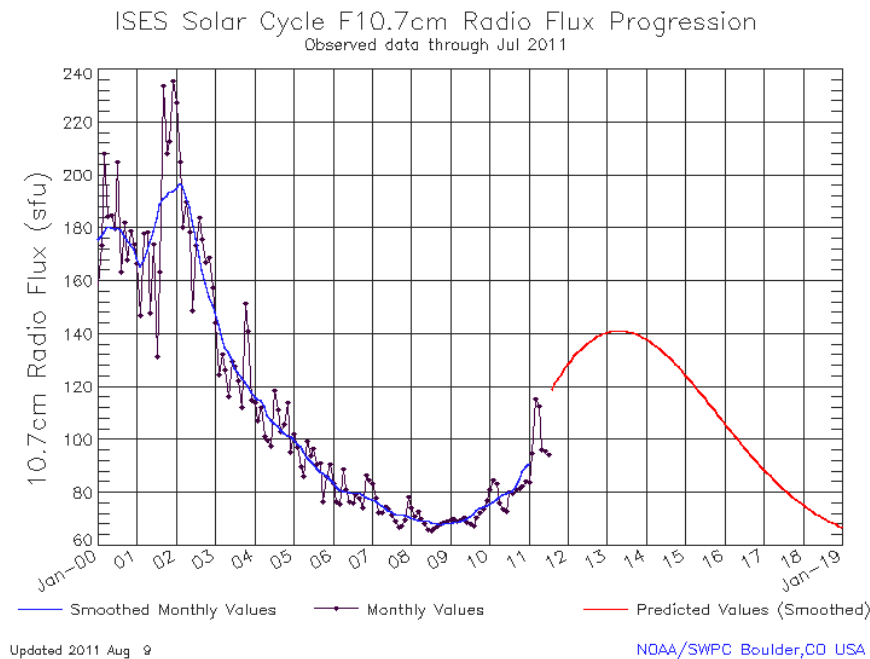


Figure 6.1: 10.7 cm Solar Radio Flux [25]

By analyzing the reference ionospheric path delay, i.e. the P1 and P2 pseudo-range combination as described by equation (4.5.9), the maximum and mean ionospheric path delay for the selected dates can be determined as can be seen in figure 6.2.

	2002-015		2002-219		2004-220		2008-315	
Max. Ionospheric delay [m] / [TECU]	129,00	79,40	191,00	117,60	170,00	104,70	81,50	50,20
Mean Ionospheric delay [m] / [TECU]	9,52	5,86	6,39	3,94	4,94	3,04	4,05	2,49

Figure 6.2: Maximum and mean ionospheric delay for the selected data sets

In agreement with figure 6.1, the selected dates show a decreasing Sun activity and thus a decreasing mean ionospheric path delay. 2002-015, at times with high solar activity, a mean ionospheric delay of 5.86 TECU was measured, whereas 2002-219 shows a value of 3.94 TECU. 2004-220 has a further decreased value of 3.04 TECU and finally 2008-315 shows the lowest mean ionospheric delay with 2.49 TECU.

The values for the maximum measured ionospheric delays are 79.4 TECU for 2002-015, 117.6 TECU for 2002-219, 104.7 TECU for 2004-220 and 50.2 TECU for 2008-315. Those values don't really show a decreasing behavior, what can be explained by the fact that solar events like solar flares, which cause these peak ionospheric values, can occur independently from the general or mean solar activity.

## 6.2 Data editing analysis

In order to decouple the effects of the implemented data editing criteria on the navigation solution from the ionospheric corrections, a first analysis is done concerning data editing. The data editing criteria as described in chapter 4.6 were applied once with the model currently implemented in the MosaicGNSS receiver, the Lear model, and once without any ionospheric corrections and then compared to the cases without data editing.

As can be seen in figure 6.3, the data editing criteria increase the accuracy of the navigation solution significantly. For times of higher solar activity the accuracy

of the navigation solution can be increased by 24 - 48 % and for times of lower solar activity by 63 - 87 %. Especially the case of the navigation solution without any ionospheric corrections is remarkable, as the data editing criteria yield to an increase in accuracy of  $\approx 80 - 87$  % in 3D position error RMS, from absolute values of 27.84 m and 16.95 m to values of 3.55 m and 3.45 m for times of low solar activity.

	3D position error RMS [m]							
	2002-015		2002-219		2004-220		2008-315	
Ionospheric Correction	original	with data editing	original	with data editing	original	with data editing	original	with data editing
Without corrections	16,92	12,10	8,56	5,06	27,84	3,55	16,95	3,45
Lear model	11,26	8,45	7,61	3,95	28,14	4,04	17,61	6,47

Figure 6.3: Influence of data editing on the navigation solution

The general effect of increased navigation solution accuracy after application of data editing criteria can be easily explained by the fact that outliers due to invalid or degraded measurements are removed effectively, thus yielding to a better quality of the measurements. The exceptional good performance of the navigation solution without ionospheric corrections but with data editing for times of low solar activity, i.e. 2004-220 and 2008-315, can be explained by the fact that outliers due to invalid or degraded measurements present the main error source in the signals, thus yielding a 3D position error that is in the order of the mean ionospheric delay. Figure 6.4 clearly shows how the global 3D position error RMS is reduced by removing outliers by means of data editing techniques.

### 6.3 Ionospheric path delay analysis

The ionospheric path delay calculated with a ionospheric correction algorithm as described in chapter 4 is compared to the reference ionospheric path delay calculated by use of P1 and P2 pseudorange measurements via equation (4.5.9).

A typical shape of the ionospheric path delay as a function of time can be seen in figure 6.5. Here, it can be observed that with increasing elevation the ionospheric

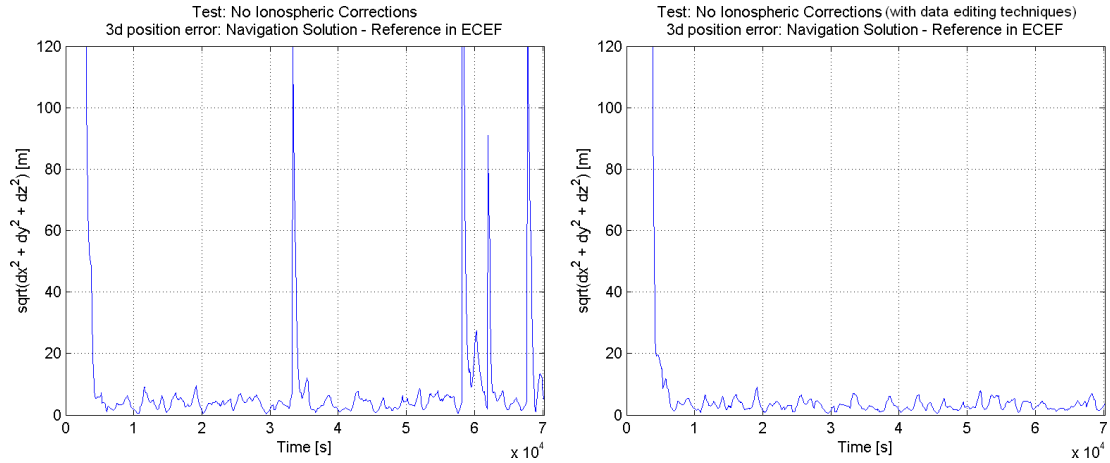


Figure 6.4: 3D position error RMS for testcase 2008-315 without data editing techniques (left) and with data editing techniques (right)

path delay basically decreases. This is in agreement with the fact that the TEC is calculated by integrating the electron density along its path through the ionosphere, hence a shorter path through the ionosphere (due to higher elevation) yields to a lower TEC and thus a lower ionospheric path delay.

The observation that the ionospheric delay is usually bigger at the end than at the beginning of a track can also be explained by a lower elevation at the end of track. This is due to the fact that when a GPS SV comes into the field of view, it takes a while until it is fully tracked, i.e. until its signal is acquired, the navigation data is obtained and the position solution is calculated, the so-called time-to-first-fix, after which the GPS SV already has an increased elevation. This explains for example the shape of the second track (middle) of figure 6.5. Here, the ionospheric delay has a value of  $\approx 2.5$  m for the begin and  $\approx 5.5$  m for the end of the track, but the elevation angle also decreases from  $\approx 30^\circ$  at the beginning to  $\approx 15^\circ$  at the end of the track

In figure 6.5 it can also be seen how the ionospheric correction algorithm (blue line), in this case the Montenbruck model, simplifies the real situation as it is shown by the reference ionospheric path delay (red line). The model resembles the shape of the reference ionospheric path delay quite well, but the magnitude has an error of approx. a factor 2.

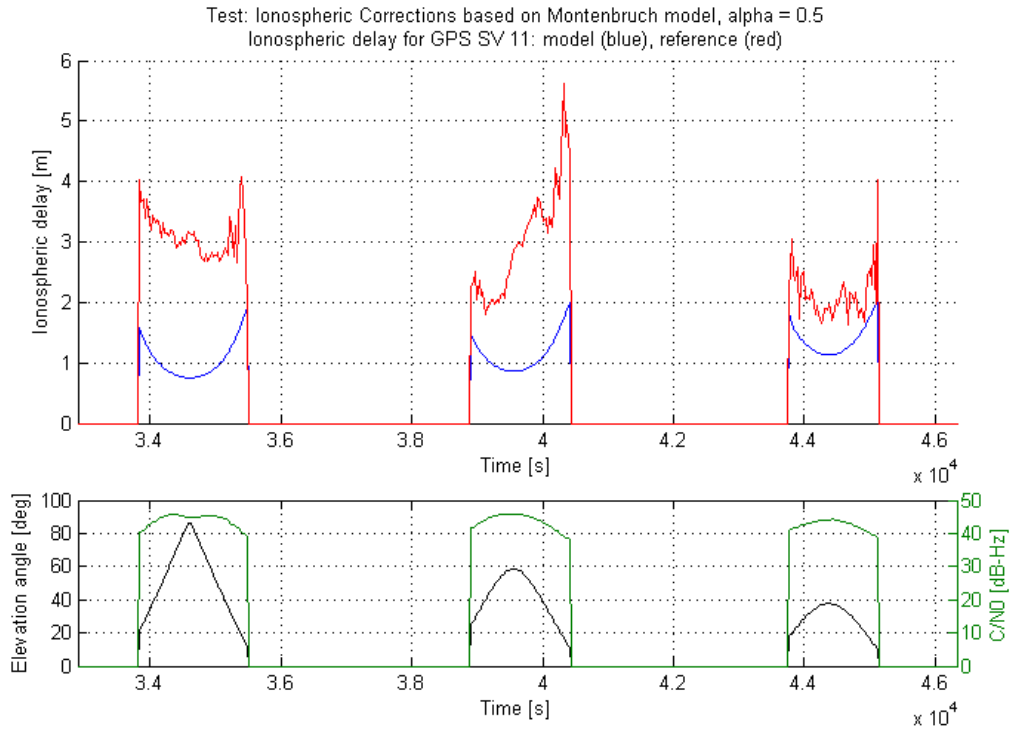


Figure 6.5: Ionospheric path delay for 3 tracks of GPS SV 11 at 2008-315. Ionospheric correction based on Montenbruck model with  $\alpha = 0.5$ . Top figure: Ionospheric path delay (model: blue, reference: red) vs. time. Bottom figure: Elevation angle (black) and carrier-to-noise density (green) vs. time

The measurement noise of the reference ionospheric path delay can also be seen very well, although the magnitude of the noise indicates for most of the time a by far lower level than the upper limit of  $\approx 2.2$  m as given in chapter 4.5. Despite the fact that the representative standard deviation for the measurement noise of a single signal in chapter 4.5 was related to C/A code (for P-code as well:  $\sigma(\epsilon) = 1$  m [24]), the measurement noise is elevation dependent and the maximum value of 1 m for the single signal is given for an elevation of  $10^\circ$  [24]. When looking at figure 6.5, one can clearly see the increase in measurement noise for low elevations, thus supporting the calculated value of  $\sigma(\epsilon) = 2.2$  m for the combined signal from chapter 4.5.

In order to have a quantitative measure of how much the calculated and reference ionospheric path delays are differing, the RMS difference for those two values is calculated. The resulting RMS differences for the different ionospheric correction algorithms for the different data sets can be found in figure 6.6.

Ionospheric correction	Delta ionospheric delay (model - reference) RMS [m]			
	2002-015	2002-219	2004-220	2008-315
Without corrections, without data editing	14,20	10,90	9,28	7,33
Without corrections, with data editing	12,60	10,30	9,34	4,84
Lear model	10,20	8,53	8,02	2,83
Lear/Klobuchar model	7,83	7,92	7,91	2,82
Montenbruck model, alpha optimized for each day	a=0,9 7,65	a=0,9 8,13	a=0,9 8,05	a=0,9 2,62
DRVID + Lear model	8,34	8,25	7,98	2,82
DRVID + Lear/Klobuchar model	9,83	8,04	7,89	3,09
DRVID + Montenbruck model (alpha = 0.5)	8,27	8,79	8,46	3,25

Figure 6.6: Comparison of ionospheric path delay differences (model - reference) for the different ionospheric correction algorithms (including data editing)

The case without any ionospheric corrections shows the capability of data editing to reduce also the ionospheric path delay by means of excluding GPS SVs with low elevations, hence with high TEC values. This yields to a reduction of ionospheric path delay of up to 2.5 m for 2008-315.

For 2002-015, the Montenbruck model with  $\alpha = 0.9$  is closest to the reference with an error of 7.65 m (compared to 14.2 m originally). The Lear model shows an error of 10.2 m and the Lear/Klobuchar combination calculated the ionospheric path delay with an error of 7.83 m. The three DRVID combinations show errors of 8.27, 8.34 and 9.83 m for the combinations with Montenbruck model ( $\alpha = 0.5$ ), Lear and Lear/Klobuchar, respectively.

For 2002-219, the Lear/Klobuchar model is the algorithm that has the least error in ionospheric path delay with a value of 7.92 m (compared to 10.9 m originally). Not far away from that value is the DRVID + Lear/Klobuchar model with 8.04 m. The Montenbruck model shows an error of 8.13 m with the optimum parameter  $\alpha = 0.9$ . The two remaining DRVID models perform with an error of 8.25 m and 8.79 m for the Lear model option and Montenbruck model ( $\alpha = 0.5$ ) option, respectively. The Lear model shows an error of 8.53 m.

The DRVID + Lear/Klobuchar combination wins for the date 2004-220 with an error value of 7.89 m, directly before the Lear/Klobuchar model with 7.91m and the DRVID + Lear combination with 7.98 m. The Lear model performs with 8.02 m and the Montenbruck model with an optimized parameter of  $\alpha = 0.9$  with 8.05 m. The DRVID + Montenbruck model (with  $\alpha = 0.5$  m) has the worst result, i.e. an error of 8.46 m.

2008-315 shows in general a low error in ionospheric path delay that is in the order of 3 m. The Montenbruck model with an optimized parameter of  $\alpha = 0.9$  again performs best with a value of 2.6 m. The Lear/Klobuchar model as well as the DRVID + Lear model show an error of 2.82 m. Close to this value is the Lear model with an error of 2.83 m. The DRVID combinations Lear/Klobuchar and Montenbruck model (with  $\alpha = 0.9$  m) perform worst with errors of 3.09 m and 3.25 m, respectively.

The tested algorithms for ionospheric correction differ in 2002-015 at most by 25 %, in 2008-315 at most by 19 % and in 2002-219 and 2004-220 at most by less than 10 %, hence they show basically similar results. The Montenbruck model shows to minimize the error in ionospheric path delay quite well due to the fact that it performs best for two out of 4 tests. The Lear/Klobuchar model shows a constant good performance by reducing the ionospheric path delay best one time and second best for the other three times.

The previous discussion is based on absolute values of the error in calculated ionospheric path delay, but attention is also paid to the shape of the calculated ionospheric path delay compared to the reference. Here, the DRVID technique in general performs best due to the fact that it shows the real shape of the ionospheric error with an accuracy even higher than the reference (see measurement noises in chapter 4.4 and 4.5).

Figure 6.7 shows a comparison between the Montenbruck model and the DRVID + Lear combination for one track of GPS SV 11 on 2008-315. On the left image one observes that the Montenbruck model approximates only the general tendency of the ionospheric path delay. Its shape doesn't show high correlation with the shape of the reference ionospheric path delay and additionally there is also a

high offset due to model deficiencies. On the right image it can clearly be seen that the shape of the ionospheric path delay of the DRVID + Lear combination resembles the reference very well. Despite the bias due to integer ambiguity, the two shapes show high correlation. For low elevations (end of track), the reduced measurement noise  $\sigma(\epsilon_c) = 0.7$  m of the DRVID + Lear combination, in contrast to the measurement noise  $\sigma(\epsilon) = 2.2$  m of the reference, can clearly be observed.

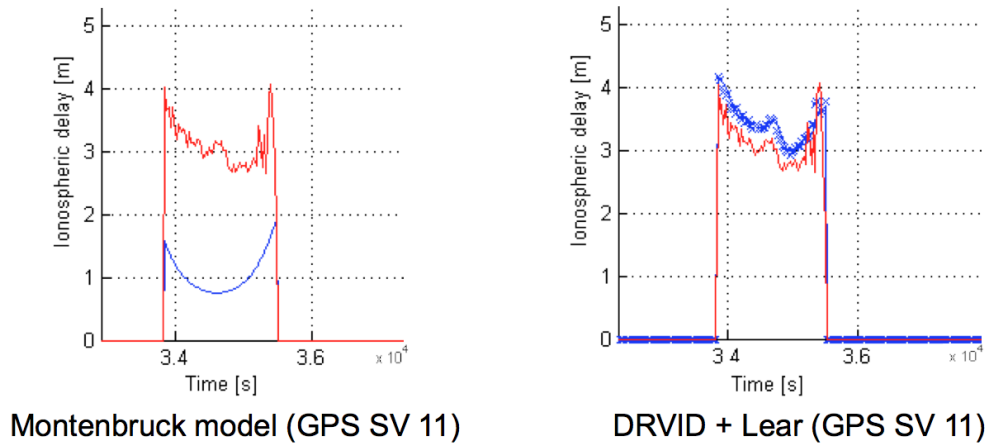


Figure 6.7: Comparison of modeled ionospheric path delay by Montenbruck model (left) and DRVID + Lear combination (right) for GPS SV 11 on 2008-315

The drawback of the DRVID technique is the need for integer ambiguity resolution that obviously can't be solved very well by means of an initialization with help of an ionospheric model, as was done in this work. Figure 6.8 shows the ionospheric path delay for 3 tracks of GPS SV 11 at 2008-315, based on DRVID + Lear ionospheric correction. It can be seen that the shape of the model (blue) fits very well to the reference shape (red). The bias due to integer ambiguity and its insufficient resolution by the Lear model can also be seen very well.

## 6.4 Navigation solution analysis

The quality of the navigation solution of the MosaicGNSS receiver is assessed by comparing the 3D position errors RMS obtained by use of the different ionospheric correction algorithms. The results can be seen in figure 6.9.

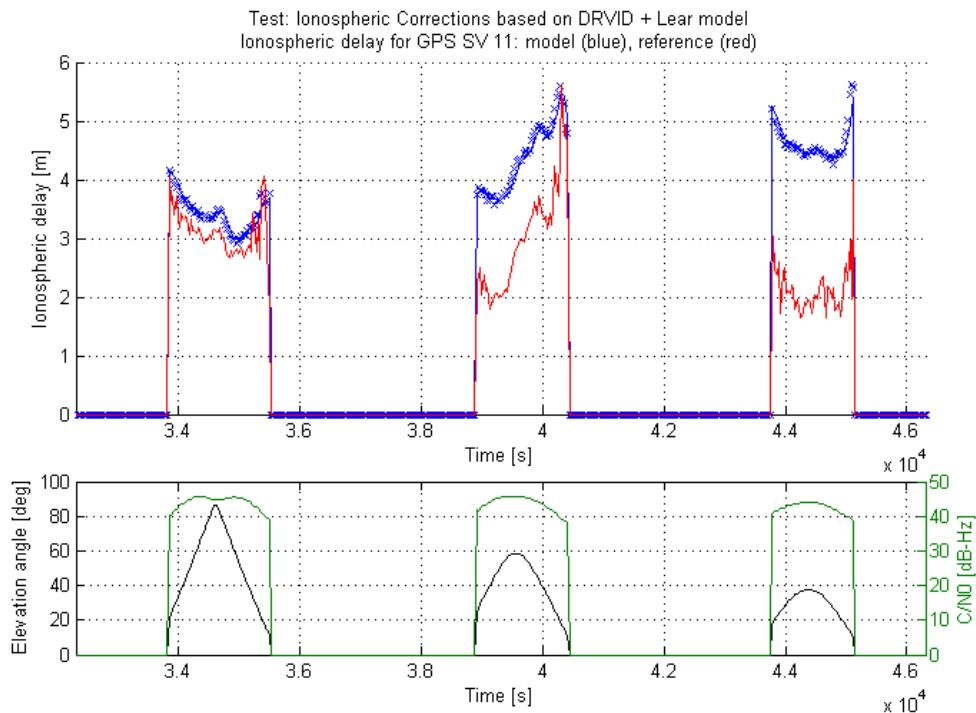


Figure 6.8: Ionospheric path delay for 3 tracks of GPS SV 11 at 2008-315. Ionospheric correction based on DRVID + Lear model. Top figure: Ionospheric path delay (model: blue, reference: red) vs. time. Bottom figure: Elevation angle (black) and carrier-to-noise density (green) vs. time

For 2002-015, the Montenbruck model with the optimized parameter  $\alpha = 0.9$  gives the best result with a 3D position error RMS of 5.6 m (compared to 16.92 m originally). The Lear/Klobuchar model performs also well with an error of 6.63 m. The Lear model and the DRVID + Montenbruck model (with  $\alpha = 0.5$ ) show resulting errors of 8.45 m and 8.88 m, respectively. The DRVID options with Lear model and Lear/Klobuchar model as basis perform with an error of 10.03 m and 13.68 m, respectively, worse than the original 10 m accuracy.

The Montenbruck model has again the lowest 3D position error RMS with 3.5 m for the 2002-219 data arc. The Lear model is again close with 3.95 m, following the DRVID + Montenbruck model (with  $\alpha = 0.5$ ) and the Lear/Klobuchar model with 4.53 m and 4.71 m, respectively. The DRVID options with Lear model and Lear/Klobuchar model perform again worst with 5.53 m and 6.43 m.

Ionospheric correction	3D position error RMS [m]							
	2002-015		2002-219		2004-220		2008-315	
Without corrections, without data editing	16,92		8,56		27,84		16,95	
Without corrections	12,10		5,06		3,55		3,45	
Lear model	8,45		3,95		4,04		6,47	
Lear/Klobuchar model	6,63		4,71		4,62		7,61	
Montenbruck model, alpha optimized for each day	a=0,9	5,60	a=0,7	3,50	a=0,5	2,96	a=0,1	3,57
DRVID + Lear model	10,03		5,53		4,43		6,31	
DRVID + Lear/Klobuchar model	13,68		6,43		4,09		6,78	
DRVID + Montenbruck model (alpha = 0.5)	8,88		4,53		3,28		4,36	
Double-frequency correction	4,86		4,72		5,80		5,60	

Figure 6.9: Comparison of 3D position errors RMS for the different ionospheric correction algorithms (including data editing)

Also for 2004-220, the Montenbruck model with an optimized parameter  $\alpha = 0.5$  shows the best navigation performance with a 3D position error of 2.96 m. The DRVID + Montenbruck model ( $\alpha = 0.5$ ) presents with an error of 3.28 m also a good result. The remaining algorithms Lear model, DRVID + Lear/Klobuchar model, DRVID + Lear model and Lear/Klobuchar model yield to errors of 4.04, 4.09, 4.43 and 4.62, respectively.

The best 3D position error RMS for 2008-315 with 3.45 m comes from the case without any ionospheric corrections but with data editing techniques, what has already been discussed in chapter 6.2. The best ionospheric correction algorithm is again the Montenbruck model with an optimized parameter  $\alpha = 0.1$  with an error of 3.57 m. The DRVID + Montenbruck model ( $\alpha = 0.5$ ) has the second best error with 4.36 m. The DRVID + Lear model, Lear model, DRVID + Lear/Klobuchar model follow with errors of 6.31 m, 6.47 m and 6.78 m, respectively.

The ionospheric correction based on double-frequency P-code measurements is considered to be the reference for the comparison of ionospheric path delays, hence one could ask why its results for the 3D position error RMS are not better. First one has to say that the ionospheric path delay calculated by the double-frequency correction is given into the navigation solution in an unsmoothed way, meaning that no low-pass-filtering was applied before. Hence, the increased measurement noise of the double-frequency combination could cause a degradation of the solution due to not well-fitting Kalman filter parameters. Secondly, the

general adjustment of the Kalman filter parameters could cause this effect as well. This is due to the fact that CHAMP GPS data was used instead of data originally recorded by the MosaicGNSS receiver. Thus the covariance settings of the MosaicGNSS receiver navigation solution may not fit to the corresponding noises in the Blackjack receiver hardware used on the CHAMP mission.

The differences in the obtained 3D position errors RMS vary by up to a factor of 2.4, emphasizing the importance of a proper selection of the ionospheric correction algorithm. Although one can't give final recommendations without a proper filter tuning in advance as described previously, the obtained values for the 3D position errors RMS from figure 6.9 can at least be seen as upper limits, which maybe become better after filter tuning. With the Lear/Klobuchar model, a maximum error of 6.63 m is obtained for 2002-015 and 2002-219, hence for times with high solar activity. At times with low solar activity, i.e. 2004-220 and 2008-315, a maximum error of 3.45 m can be achieved by using no ionospheric corrections but only the newly developed data editing techniques. This yields to the idea of switching (via telecommand) to a ionospheric correction algorithm corresponding to the long-term solar activity. In this sense it is proposed to use the Lear/Klobuchar model for times of high solar activity and totally switch off the ionospheric corrections for times of low solar activity. A prerequisite for this is of course that for both cases the newly developed data editing techniques as described in chapter 4.6 are enabled. With this strategy, a 3D position error RMS of 3.45 - 6.63 m can be achieved for both times with high - and low solar activity. A filter tuning under consideration of both the cases should be done as well as to further analyze the stability and performance of the navigation solution.

The Montenbruck model hasn't been mentioned as recommended algorithm although it performed best for 3 out 4 cases due to the fact that its parameter  $\alpha$  has to be adapted to the current situation of the ionosphere. In the tests performed during this work, the parameter  $\alpha$  has been determined in a post-processing manner (brute-force search), which is of course no option for a real-time navigation system. The estimation of this parameter via models also doesn't seem to be very handy for real-time applications. Hence, the way of implementing a sequential batch filter to determine the parameter  $\alpha$  has to be gone, if one wants to increase the accuracy effectively, what also means that the restrictions of changing as little

code as possible most likely have to be given up. Looking at the results in figure 6.9 with roughly determined values of  $\alpha$  that give 3D position errors of 2.96 - 5.6 m lets this idea become promising, thus further research in that direction should be done.

The GRAPHIC code / DRVID technique doesn't perform as well as expected. Estimating the bias by help of ionospheric models didn't show satisfying results in the 3D position error RMS, what is either related to not well-fitting Kalman filter parameters or more likely to the fact that the navigation filter performs poorly with a constant error, i.e. the bias that remains after the estimation process. Due to the fact that by using the GRAPHIC code / DRVID technique one shall be able to obtain 3D position errors comparable with double-frequency corrections [12], it should be considered to think about the possibility of giving up the restriction of changing as little code as possible and instead implementing an integer ambiguity resolution technique.

## Concluding remarks

In this work, several ionospheric correction algorithms as well as some basic data editing techniques were developed, implemented and tested and finally validated by use of real flight data from the CHAMP mission.

Regarding the magnitude of the ionospheric path delay, the tested algorithms for ionospheric correction differ in 2002-015 at most by 25 %, in 2008-315 at most by 19 % and in 2002-219 and 2004-220 at most by better than 10 %, hence showing basically similar results. The Montenbruck model shows to minimize the error in ionospheric path delay quite well due to the fact that it performs best for two out of four tests. The Lear/Klobuchar model shows a constant good performance by reducing the ionospheric path delay best one time and second best for the other three times. Concerning the shape of the ionospheric path delay, the GRAPHIC code / DRVID technique performs best, it shows the real shape of the ionospheric error with an accuracy even higher than the reference used for this work.

Concerning the navigation solution of the MosaicGNSS receiver, the differences in the obtained 3D position errors RMS vary by up to a factor of 2.4, hence emphasizing the importance of a proper selection of the ionospheric correction algorithm. Although a final recommendation can only be given after a proper filter tuning, a first proposal for the selection of ionospheric correction algorithms for the MosaicGNSS receiver can be done. The differing 3D position accuracy for the ionospheric correction algorithms concerning high - and low solar activity leads to the idea of switching (via telecommand) to a ionospheric correction algorithm corresponding to the long-term solar activity. In this sense, it is proposed to use the Lear/Klobuchar model for times of high solar activity and totally switch off the ionospheric corrections for times of low solar activity. A prerequisite for this is of course that for both cases the newly developed data editing techniques are enabled. With this strategy, a 3D position error RMS of 3.45 - 6.63 m can be achieved for both times with high - and low solar activity. When comparing these

values with the original 3D position error RMS of 10 m, an increase in accuracy of 33 % to 65 % is obtained.

Future work should be done on implementing and testing the Montenbruck model with a sequential batch filter that determines the scaling parameter  $\alpha$  autonomously. Additionally, for the GRAPHIC code / DRVID technique, a technique for integer ambiguity resolution should be implemented and tested in order to properly account for the bias.

# References

- [1] Montenbruck O., Gill E., 2001, "Satellite orbits: Models, Methods, Applications", corrected 2nd printing, Springer Verlag Berlin Heidelberg New York
- [2] Wertz, James R. and Larson, Wiley J., 1999, "Space Mission Analysis and Design", 3rd edition, Microcosm Press and Springer
- [3] EADS Astrium, 2009, Product description "MosaicGNSS Receiver, GPS receiver as Slide-In Module for LEO, MEO and GEO", internal id: 8244MN 01.03.10
- [4] EADS Astrium, 20.04.2010, "MosaicGNSS Receiver, Navigation Algorithms, Top Level Description", internal id: MosiacGNSS-176-110
- [5] Montenbruck O., Garcia-Fernandez, M., 2005, "Ionospheric Path Delay Models for Spaceborne GPS", DLR, DLR-GSOC TN 05-07, issue 2005/11/2
- [6] EADS Astrium, 28.05.2010, "Feasibility of GNSS Sensors for AOCS Applications in GEO and Higher Altitudes, D4: Simulator Design Description (including Physical Model and Onboard Algorithms) and User Manual", internal id: GNSS\_GEO\_TN\_04, issue 2.0
- [7] Spirent Communications, 2009, "GSS8000 Series, GNSS Constellation Simulator", MCD00128 10/09
- [8] Spirent Communications, December 2009, "SIMGEN Software User Manual", DGP00686AAA, issue 1-36
- [9] Klobuchar J. A., 1987, "Ionospheric Time-Delay Algorithm for Single-Frequency GPS Users", IEEE Transactions on Aerospace and Electronic Systems, Vol. AES-23, No. 3
- [10] Klobuchar J. A., 2001, "Eye on the Ionosphere: Correction Methods for GPS Ionospheric Range Delay", GPS Solutions, Vol. 5, No. 2, pp. 91-92
- [11] Krauss P. A. et al., 2010, "New Applications for Navigation Receivers in Space", 5th ESA Workshop on Satellite Navigation Technologies (NAVITEC)

- 2010) and European Workshop on GNSS Signals and Signal Processing, ESTEC, Noordwijk
- [12] Montenbruck O., 2003, "Kinematic GPS positioning of LEO satellites using ionosphere-free single frequency measurements", *Aerospace Science and Technology*, 7 (2003) 396-405
- [13] Montenbruck O., Gill E., 2002, "Ionospheric Correction for GPS Tracking of LEO Satellites", *The Journal of Navigation*, Vol. 55, 293-304
- [14] Parkinson B.W. et al., 1996, "Global Positioning System: Theory and Applications, Volume I", 3rd printing, Volume 163, *Progress in Astronautics and Aeronautics*
- [15] Montenbruck O., Ramos-Bosch P., 2007, "Precision real-time navigation of LEO satellites using global positioning system measurements", *GPS Solut* (2008), 12:187-198
- [16] Global Positioning System Wing, Systems Engineering & Integration, 2000, "Interface Specification IS-GPS-200, Revision E", <http://www.gps.gov/technical/icwg/IS-GPS-200E.pdf>, as of 01.09.2011 14h
- [17] Tribble A.C., 2003, "The Space Environment: Implications for Spacecraft Design", Princeton University Press
- [18] Goldstein D.B., 2000, "Real-time, Autonomous, Precise Satellite Orbit Determination using the Global Positioning System", PhD thesis, University of Colorado at Boulder
- [19] GFZ German Research Centre for Geosciences, "CHAMP: Mission and Orbit", [http://www-app2.gfz-potsdam.de/pb1/op/champ/orbit/index\\_PRD.html](http://www-app2.gfz-potsdam.de/pb1/op/champ/orbit/index_PRD.html), as of 01.09.2011 14h
- [20] CHAMP ISDC, "CHAMP project", <http://isdc.gfz-potsdam.de/index.php?module=pagesetter&func=viewpub&tid=1&pid=34>, as of 01.09.2011 14h
- [21] Gurtner W., "RINEX: The Receiver Independent Exchange Format Version 2.10", <http://www.ngs.noaa.gov/CORS/Rinex2.html>, as of 01.09.2011 14h

- [22] GFZ German Research Centre for Geosciences, "RINEX format observable extensions for CHAMP SST Data", [http://op.gfz-potsdam.de/champ/docs\\_CHAMP/CH-RINEX-EXT.html](http://op.gfz-potsdam.de/champ/docs_CHAMP/CH-RINEX-EXT.html), as of 01.09.2011 14h
- [23] GFZ German Research Centre for Geosciences, "Format Description: The CHAMP Orbit Format", [http://op.gfz-potsdam.de/champ/docs\\_CHAMP/CH-GFZ-FD-002.pdf](http://op.gfz-potsdam.de/champ/docs_CHAMP/CH-GFZ-FD-002.pdf), as of 01.09.2011 14h
- [24] Gill E., Montenbruck O., 2004, "Comparison of GPS-based Orbit Determination Strategies", 18th International Symposium on Space Flight Dynamics, 11.-15.10.2004, München, Germany
- [25] NOAA / Space Weather Prediction Center, "Solar Cycle Progression", <http://www.swpc.noaa.gov/SolarCycle/>, as of 01.09.2011 14h
- [26] Kühl C.T.F., 2005, "Combined earth-/star sensor for attitude and orbit determination of geostationary satellites", PhD thesis, University of Stuttgart
- [27] Zentgraf P. et al., 2010, "Preparing the GPS Experiment for the Small Geo Mission", 33rd Annual AAS Guidance Navigation & Control Conference, February 6-10, 2010, Breckenridge, Colorado

# List of figures

1.1	Time schedule for Master thesis . . . . .	3
2.1	Order of magnitude of various perturbations of a satellite's orbit [1]	5
2.2	Altitude vs. electron density for day/night - and solar activity variation [17] . . . . .	10
2.3	"Monthly averages of the solar flux for solar cycles 20-23." [1] . .	11
4.1	Geometry of the Montenbruck model [13] . . . . .	23
6.1	10.7 cm Solar Radio Flux [25] . . . . .	35
6.2	Maximum and mean ionospheric delay for the selected data sets .	36
6.3	Influence of data editing on the navigation solution . . . . .	37
6.4	3D position error RMS for testcase 2008-315 without data editing techniques (left) and with data editing techniques (right) . . . .	38
6.5	Ionospheric path delay for 3 tracks of GPS SV 11 at 2008-315 . .	39
6.6	Comparison of ionospheric path delay differences . . . . .	40
6.7	Comparison of modeled ionospheric path delay by Montenbruck model (left) and DRVID + Lear combination (right) for GPS SV 11 on 2008-315 . . . . .	42
6.8	Ionospheric path delay for 3 tracks of GPS SV 11 at 2008-315 . .	43
6.9	Comparison of 3D position errors RMS . . . . .	44